SYNTHESIS AND CHARACTERIZATION OF NANOSTRUCTURED POLYANILINE SUPPORTED g–C_3N_4/ZnO/CeO_2 SENSOR FOR MALATHION DETECTION

MSc THESIS

FANTAHUN GONFA ABDETA

JUNE 2018

HARAMAYA UNIVERSITY, HARAMAYA

Synthesis and Characterization of Nanostructured Polyaniline Supported g–C_3N_4/ZnO/CeO_2 Sensor for Malathion Detection

A Thesis Submitted to the Department of Chemistry, Postgraduate Program Directorate

HARAMAYA UNIVERSITY

In partial Fulfillment of the Requirements for the Degree of

MASTER OF SCIENCE IN CHEMISTRY (INORGANIC)

Fantahun Gonfa Abdeta

June 2018

Haramaya University, Haramaya

HARAMAYA UNIVERSITY

POSTGRADUATE PROGRAM DIRECTORATE

I hereby certify that I have read and evaluated this Thesis entitled **''Synthesis and Characterization of Nanostructured Polyaniline Supported g–C_3N_4/ZnO/CeO_2 Sensor for Malathion Detection''** prepared under my guidance by Fantahun Gonfa. I recommend that it be submitted as fulfilling the thesis requirement.

Abi Taddesse (PhD)	_____	_____
Major Advisor	Signature	Date
Abebaw Adgo (PhD)	_____	_____
Co-Advisor	Signature	Date
Isabel Diaz (Prof.)	_____	_____
Co-Advisor	Signature	Date

As a member of the Board of Examiners of the MSc Thesis Open Defense Examination, I certify that I have read and evaluated the thesis prepared by Fantahun Gonfa and examined the candidate. I recommend that the thesis be accepted as fulfilling the Thesis requirement for the degree of Master of Science in Chemistry (Inorganic Chemistry).

_____	_____	_____
Chairperson	Signature	Date
_____	_____	_____
Internal Examiner	Signature	Date
_____	_____	_____
External Examiner	Signature	Date

DEDICATION

I dedicate this thesis manuscript to my father Gonfa Abdeta and my mother Bultu Arfasa, for nursing me with affection, love and for their dedicated partnership to the success of my life.

STATEMENT OF THE AUTHOR

By my signature below, I declare and affirm that this Thesis is my own work and I have followed all ethical and technical principles of scholarship in the preparation, data collection, data analysis and complication of this thesis. Any scholarly matter that is included in the Thesis has been given recognition through citation.

This Thesis is submitted in partial fulfillment of the requirements for MSc Degree in Inorganic Chemistry at Haramaya University. The Thesis is deposited in the Haramaya University Library and is made available to borrowers under the rules of the Library. I solemnly declare that this Thesis has not been submitted to any other institution anywhere for the award of any academic degree, diploma or certificate.

Brief quotations from this Thesis may be made without special permission provided that accurate and complete acknowledgment of source. Requests for extended quotations from or reproduction of this Thesis in whole or in part may be granted by Head of the Department or Directorate of PGPD when in his or her judgment the proposed use of the material is in the interests of scholarship. In all other instances, however, permission must be obtained from the author of the Thesis.

Name: Fantahun Gonfa Signature: _____

Date: _____

Department: Chemistry

BIOGRAPHICAL SKETCH OF THE AUTHOR

The author was born in Agaro, Ethiopia, on March 19, 1994. He attended his elementary and junior education from 2000 – 2007 in Komba and Rasdesta Damitew Agaro Elementary Schools and secondary and preparatory education at Agaro Secondary and Preparatory School. After completing preparatory school, he then joined Gondar University, Department of Chemistry in 2012 and graduated with B.Sc. Degree in Chemistry in 2015. Soon after graduation, he joined the Postgraduate Program Directorate of the Haramaya University as a candidate for Master of Science in Chemistry (Inorganic Chemistry), under the regular postgraduate program.

ACKNOWLEDGEMENTS

I would like to take this opportunity to first and foremost thank God for being my strength. Without Him, I would not have had the wisdom or the physical ability to do so. The Almighty has given me the power to believe in my passion and pursue my dreams. I could never have done this without the faith I have in you.

I express my gratitude to my thesis advisors Dr. Abi Taddesse and Dr. Abebaw Adgo for devoting much time to reading my work over and over again. Their special interest and knowledge on synthesis of nanomaterials and sensor application enabled them to give me the right guidance and also provided me with much needed motivation.

I also would like to extend my acknowledgement to Dr. Endale Teju for providing me many materials and share so many hours of encouraging and invaluable advice with no reservation and insight throughout my studies. Besides, I also appreciate his critical comments and constructive criticism given to me.

I would like to acknowledge all the academic and technical staff members of the Department of Chemistry, Haramaya University, for their support especially Dr. Ephrem Tadesse, Mr. Zewudu Bezu and Mr. Samuel Chufamo who made the materials for my work easily accessed. I would like to extend my deepest gratitude to my friends, Dawit Alemu and Temesgen Girma for their help, support throughout the study period.

I gratefully acknowledge the Ministry of Education, for facilitating the financial requirements. I also acknowledge Addis Ababa University, Chemistry Department and Instituto de Catálisis Y Petroleoquímica, CSIC, C/Marie Curie 2, Madrid, Spain for their cooperation in characterizing the nanomaterials.

Finally, I must express my very profound gratitude to my family for providing me with unfailing support and continuous encouragement throughout my years of study and through the process of researching and writing this thesis.

ACRONYMS AND ABBREVIATION

BET	Brunauer–Emmett–Teller
CN	Carbon nitride
CV	Cyclic voltammetry
DPV	Differential pulse voltammetry
EIS	Electrochemical impedance spectroscopy
FTIR	Fourier transform infrared spectroscopy
GCE	Glassy carbon electrode
LOD	Limit of detection
NPs	Nanoparticles
PANI	Polyaniline
PBS	Phosphate buffer solution
PBS	Phosphate buffer solution
RSD	Relative standard deviations
SEM	Scanning electron microscope
TGA	Thermogravimetric Analysis
UV-Vis	Ultraviolet-Visible spectroscopy
XRD	X-ray diffraction

TABLE OF CONTENTS

LIST OF TABLES

Table **Page**

LIST OF FIGURES

Figure **Page**

LIST OF TABLES IN THE APPENDIX

Appendix Table **Page**

SYNTHESIS AND CHARACTERIZATION OF NANOSTRUCTURED POLYANILINE SUPPORTED g–C_3N_4/ZnO/CeO_2 SENSOR FOR MALATHION DETECTION

ABSTRACT

In this study, PANI/g–C_3N_4/ZnO/CeO_2 modified glassy carbon electrode (GCE) electrochemical sensor was developed for the detection of malathion. The structure, optoelectronic properties, surface functional groups, morphology, thermal stability and surface area of the nanocomposites were characterized by X-ray diffraction (XRD), UV-Vis spectroscopy, Fourier transform infrared (FTIR), Scanning electron microscopy (SEM), Thermogravimetric Analysis (TGA) and BET analysis. Cyclic voltammetry (CV) and electrochemical impedance spectroscopy (EIS)) were used to investigate the electrochemical behavior GC modified electrode by the various as produced nanocomposite in the presence of 2 mM $K_3Fe(CN)_6$/0.1 M KCl and 0.1 M phosphate buffer(PBS). The recorded voltammogram indicated that enhanced electrochemical signal was observed in the case of PANI/g–C_3N_4/ZnO/CeO_2/GC electrode. Besides, the same electrode showed smaller charge transfer resistance as noticed from EIS spectra. These could be most probably due to contributions coming from the high conductivity of g–C_3N_4 and catalytic effect of both ZnO and CeO_2. To improve the performance of PANI/g–C_3N_4/ZnO/CeO_2/GCE sensor for the detection of malathion, pH of PBS solution and scan rate were optimized. Under optimized experimental conditions (pH = 7.0 and = 50 mVs^{-1}) the concentration of malathion in standard solutions from 2.0 × 10^{-8} to 14.0 × 10^{-8} M was determined using differential pulse voltammetry. The sensor exhibited a linear range 2.0 × 10^{-8} to 14.0 × 10^{-8} M, sensitivity 11.85 μA/μM and low detection limit of 10.94 × 10^{-9} M. In addition to this, PANI/g–C_3N_4/ZnO/CeO_2/GCE sensor was applied to determine the level of malathion in khat. The findings demonstrated that the sensor developed from these nanomaterials can be a good candidate for the non-enzymatic determination of malathion in various samples.

Keywords*: Carbon nitride, Cerium dioxide, Malathion, Nanocomposite, Polyaniline, Zinc oxide*

1. INTRODUCTION

Food and Drug Administration (FDA) reports about 1045 chemicals as pesticide residues (FEPA, 2004). Pesticides are chemical substances applied to crops at various stages of cultivation and during the post-harvest storage of crops. The use of pesticides is intended to prevent the destruction of food crops by controlling agricultural pests or unwanted plants and to improve plant quality (Bakirci and Hisil 2011). Pesticide use in commercial agriculture has led to an increase in farm productivity. Despite the wide ranging benefits of using pesticides in agriculture, several incorrect applications can result in high and undesirable levels of the compounds in the produce that reaches consumers (Chen *et al*., 2011).

Ethiopia is one of the African countries that use different kinds of pesticides for agricultural, industrial and health care purposes. Pesticides are mainly imported for agricultural purposes while some amounts of pesticides are imported for health care and industrial purposes. Large quantities of pesticides are imported annually to Ethiopia. In this regard, over 3000 tons of various types of pesticides worth more than USD 20 million are imported annually (FEPA, 2004). Ethiopia is not only importer of these agrochemicals but also produces some of them locally in Adami Tulu. The plant has a capacity to formulate 1500 tons of dust and the same quantity liquid formulations every year. Major pesticide formulated include, Malathion, (Ethiolation 5% Dust and Ethiolathion 50% EC), Endosulfan (Ethiosulfan 25% ULV), Diazinon (Ethiozinone 60% EC), and Fenithrothion (Ethiothrothion 50% EC).

Several techniques such as chromatography, capillary electrophoresis, electrochemistry, mass spectrometry, Fourier transform infrared (FTIR) detection, various spectroscopic, and colorimetric assays, have already been employed to detect pesticides in biological and pharmaceutical samples (Guan *et al*., 2010; Simsikova *et al*., 2014). Although these methods offer quantitative analysis with sensitivity and selectivity, they are slow, expensive, laborious and not convenient to popularize and promote. Moreover, they don't have the ability of information sharing and remote control. Therefore, they are not suitable for rapid detection and agricultural products traceability (Pérez-López and Merkoci 2011). Furthermore, they are costly and/or rely upon sophisticated instruments and skilled manpower, making these approaches impractical for regular environments and food safety monitoring. The fact that

none of these existing methods can provide specific results which could be used to establish rapid diagnoses means that the development of new methods of detection is still of great interest.

Great progress has recently been made in applying nanomaterials to sensor and biosensor development (Aragay *et al.*, 2011). Owing to the properties afforded by the small size of nanomaterials; their large surface to volume ratios; their physicochemical properties, composition, and shape; and their unusual target binding characteristics, these sensors can markedly improve the sensitivity and specificity of analyte detection. Said properties, together with the overall structural robustness of nanomaterials, make these materials highly amenable for use in various detection schemes based on diverse transduction modes. An explosion of research in this field has yielded myriad approaches to pesticide detection and degradation systems employing various kinds of nanomaterials, including metal nanoparticles (NPs), carbon nanotubes (CNTs), graphene, magnetic nanoparticles, and/or quantum dots (Zhang and Fang 2010). Nanosensors for pesticide residue detection offer, high sensitivity, low detection limits, super selectivity, fast responses, and small sizes (Liu *et al*., 2008).

Nanostructured metal oxide semiconductors possess high surface area, nontoxicity, good biocompatibility, catalytic activity, chemical stability. They have been investigated for various applications such as solar cells, electrochemistry sensors and biosensor. Among the metal oxide semiconductors, zinc oxide (ZnO) is considered to be one of the most popular sensing materials because of its large excitation energy, excellent electronic and photonic properties (Singh *et al*., 2014). Many efforts have been devoted to obtain high sensing performance for ZnO sensing materials. In the past decade, ZnO nanomaterials with various morphologies have been synthesized, such as nanowires, nanotubes, nanobelts, microspheres, hierarchical nanostructures, etc. because the morphology and structure can largely affect the performances of the sensing materials (Wu *et al*., 2016).

Noble metal modification is an effective method to improve the sensing performance. It is known that noble metal nanoparticles, such as Au, Ag and Pt nanoparticles, are high-effective oxidation catalysts. Therefore, the modified noble metal nanoparticles would greatly improve the response and selective properties of the ZnO materials for their exceptional catalytic activities.

Formation of heterostructures is another approach to enhance the sensing ability of ZnO. In sensing field, as it is well known, a depletion layer or an accumulation layer will form at the interfaces of the heterojunctions under the equilibrium condition, in which the transfer of the carriers can be facilitated or restrained, resulting in the enhanced sensing properties of the sensor (Saboor *et al*., 2017). Up to now, variety of semiconductor-semiconductor nano-heterostructure materials (for instance, TiO_2-ZnO, CuO-ZnO, CeO_2-ZnO and SnO_2-ZnO etc.) (Wang *et al*., 2017) have been extensively investigated for their application in the sensing field, and inspiring accomplishments have been achieved. Therefore, establishing heterostructures in sensing materials has long been regarded as the best strategy to design high-performance gas sensors. In view of this fact, the current research focuses on the fabrication of heterostructured chemosensor with ZnO, CeO_2, g–C_3N_4 components and polyaniline as a support. Polyaniline (PANI) is one of the popular conjugated semiconducting polymers which is used in the varieties of application like, optoelectronics, bio-sensors, gas sensors, electrochemical sensors, microelectronics etc., due to its high chemical stability, simple polymerization, and the high conductivity (Ameen *et al*., 2016).

Recently, doped and composite lanthanide oxide materials have been explored extensively for a variety of applications. Ceria (CeO_2) is one of the most studied oxide among the various lanthanide oxides owing to its excellent mechanical strength, high oxygen storage capacity (OSC), good optical properties, high conductivity, good redox performances, high specific surface area particularly in nano regime, high thermal stability, abundance of active sites and oxygen vacancies on the surface, and most importantly low cost synthesis (Ahmad *et al*., 2016). These properties make this material a promising candidate for a number of applications. The performance of these properties, and hence the versatility for potential applications can be enhanced by either doping or making its composites with other metals or metal oxides. Transition metal like Ni, Cu, Zn, Co, Sc, Y, Zr, Ti, Fe and metal oxides such as ZnO, TiO_2, CuO, CaO, NiO, Tb_2O_3, MnO_2 etc. are some of the reported examples of dopants and additive materials, respectively for CeO_2. Doped or composite CeO_2 materials are potentially used as photocatalysts, electrochemical sensors, gas sensors, biosensors, anodic materials for fuel cells and lithium ion batteries, super-capacitors, catalyst for CO oxidation, electrochemical charge storage devices and many more. Singh *et al*. (2014) successfully synthesized well crystalline CeO_2–ZnO nano-ellipsoids via facile hydrothermal process at

low-temperature conditions. These nano-ellipsoids exhibited a high sensitivity of approximately 0.120 μA/μMcm^2 with a low detection limit of 1.163 μM for 4-nitrophenol.

Graphitic carbon nitride (g–C_3N_4), a two-dimensional (2D) planar conjugation material, has large surface area and good chemical stability, and most importantly, it can be easily combined with other compounds by ultrasonic dispersion method, deposition-precipitation method and so on. The g–C_3N_4 with a band gap of 2.7 eV is suitable to implement a host/guest n/n junction architecture with other metal oxides of appropriate flat band potentials to effect electron transfer. In addition, because of its high nitrogen content, g–C_3N_4 can provide more active reaction sites than the other CN material, and its lamellar structure benefits the transport of electron. g–C_3N_4 has been extensively applied in sensing (Cheng *et al*., 2013), drug delivery (Lin *et al*., 2014), imaging (Zhang *et al*., 2014), and environmental applications (Sierra *et al*., 2016) owing to its unique features.

Up to now, variety of nanosensors based on ZnO, CeO_2, and g–C_3N_4 nanomaterials were developed. Zhai *et al* 2018, Singh *et al.*, 2014, and Xu *et al.*, 2016 prepared g–C_3N_4/ZnO, ZnO/CeO_2, and g–C_3N_4 for the detection of ethanol, 4-nitrophenol, and Pyrophosphate respectively. To the best of the researcher's knowledge, no work is reported so far with regard to the supported ternary system PANI/g–C_3N_4/ZnO/CeO_2 nanocomposite for sensor application. In this work, a novel PANI/g–C_3N_4/ZnO/CeO_2 sensor was prepared, and characterized to investigate its detection capacity for malathion as a target pollutant.

Objectives of the Study

General Objective;

To develop Polyaniline supported g–C_3N_4/ZnO/CeO_2 sensor for determination of malathion.

Specific Objectives;

- To synthesize PANI/ZnO, PANI/g–C_3N_4/ZnO, PANI/CeO_2/ZnO and PANI/g–C_3N_4/ZnO/CeO_2 nanomaterials.
- To characterize the structural and morphological properties of PANI/ZnO, PANI/CeO_2/ZnO, PANI/g–C_3N_4/ZnO, and PANI/g–C_3N_4/ZnO/CeO_2 nanomaterials by using XRD, TGA/DTA, SEM, BET, FTIR, and UV–Vis spectrometer.
- To construct and characterize PANI/ZnO/GCE, PANI/g–C_3N_4/ZnO/GCE, PANI/CeO_2/ZnO/GCE and PANI/g–C_3N_4/ZnO/CeO_2/GCE sensors by using CV and EIS.
- To optimize parameters of pH and scan rate.
- To apply PANI/g–C_3N_4/ZnO/CeO_2/GCE sensor for detection of trace level of malathion in khat sample by using differential pulse voltammeter.

2. LITERATURE REVIEW

2.1. Organophosphate Pesticide

Organophosphate pesticides constitute a heterogeneous category of chemicals specifically designed for the control of pests, weeds or plant diseases. These compounds (OPCs) are significant environmental and food chain pollutants due to their intensive use as pesticides in agriculture. Other important sources of such pollutants are manufacturing sites, spills during their transportation, and inappropriate use and storage. Chemicals of this group are also the basis for several different chemical weapons and a potential source of serious environmental problems due to deliberate use, accidents, or improper disposal. However their application is still the most effective and accepted means for the protection of plants, and has contributed significantly to enhanced agricultural productivity and crop yields (Bolognesi 2003).

Organophosphates (OP) are used as insecticides in agricultural and domestic settings throughout the world. As nerve agents, they have also been used in warfare and terrorist attacks. The mechanism of action is through the inhibition of the enzyme acetylcholinesterase, leading to the accumulation of acetylcholine at cholinergic synapses. The excess acetylcholine causes constant acetylcholine receptor triggering, resulting in malfunction of the autonomic, somatic and central nervous systems (Aardema *et al.,* 2008). The fundamental structure of organophosphorus pesticides is:

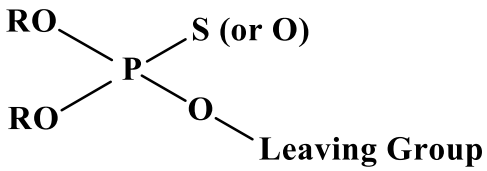

Figure 1. General chemical composition of organophosphate pesticides

The OPs are a group of both synthetic and biogenic OP compounds, characterized by the presence of the binding covalent, carbon to phosphorus (C–P) bond. In OPs, this carbon to phosphorus bond replaces one of the four carbon-to-oxygen-to-phosphorus bonds of the more common phosphate ester. While the vast majority of phosphorus-containing organic compounds contain the phosphate ester bond, both synthetic and naturally occurring

phosphonates are still of importance. The direct C–P linkage is chemically and thermally inert, with the result, most of organophosphonate compounds are resistant to chemical hydrolysis, thermal decomposition and photolysis compared with analogous compounds containing the more reactive N–P, S–P or O–P linkages (Wanner and Metcalf, 1992).

2.1.1. Malathion

Malathion is an organophosphorus insecticide used in public health, residential, and agricultural settings as early as 1950. The chemical name of malathion is dimethyl phosphorothiolothionate and its molecular formula is $C_{10}H_{19}O_6PS_2$. Malathion is widely used in agriculture, residential landscaping, and public recreation areas and in public health pest control programs such as mosquito eradication. According to World Health Organization, every year there are three million pesticide poisonings, mostly OP–related, and 200,000 deaths worldwide that are attributed either as self-poisoning or occupational exposure. Besides human exposure, there is also concern that these pesticides could leak into ground and municipal water supplies and pollute surrounding environment (Bird *et al.,* 2008).

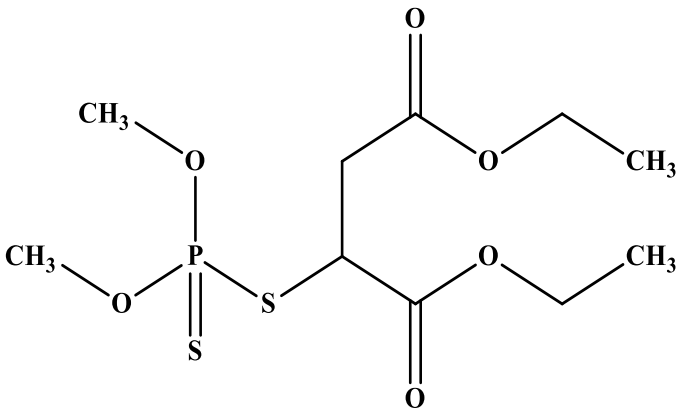

Figure 2. Chemical structure of malathion

Malaoxon is an oxygen analogue of malathion and it can be found either as an impurity in malathion product, or can be generated during the oxidation of malathion in air or soil. Malaoxon is the active cholinesterase inhibiting metabolite of malathion. Both malathion and malaoxon are detoxified by carboxyesterases to polar, water-soluble compounds that are excreted.

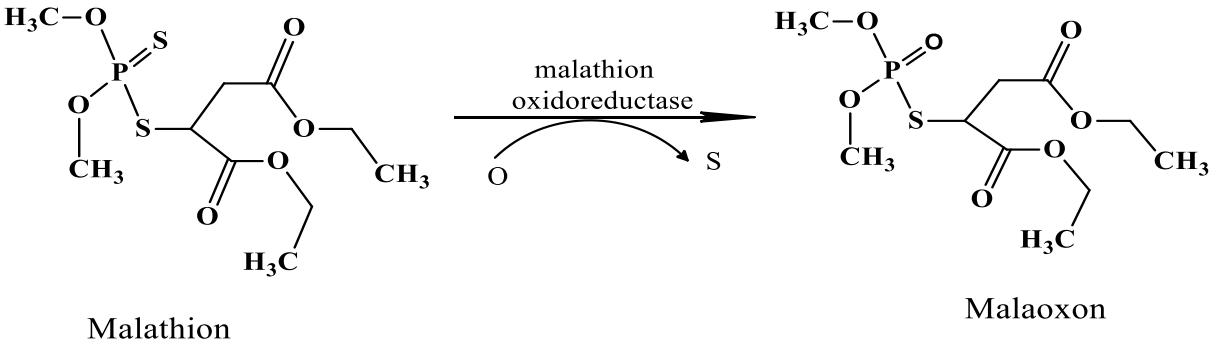

Figure 3. Oxidation process of malathion

2.2. Organophosphate Pesticides Detection Techniques

2.2.1. Chromatographic Techniques

Chromatographic techniques are the most commonly used methods for determination of OPCs. These techniques allow selective and quantitative determination. However, they have a number of disadvantages: (i) the currently available equipment is complex and expensive, which prohibits use for rapid analyses under field conditions; (ii) the pretreatment and assay procedures are lengthy, hence fast analyses are impossible; (iii) the techniques are expensive and can only be performed by highly trained technicians. Environmental issues require far more sensitive, selective, and quantitative methods, capable of low-level OPCs detection under field conditions in streams, ground, and waste waters, soils, and plants as well as in food (Rogers 1995).

2.2.2. Spectrophotometric Techniques

This was a widely used method for the detection of pesticide residues from environmental samples. Spectrophotometric detection methods were also found suitable for detection of organopesticides such as malathion, phorate and dimethoate from food samples. Hernández *et al.*, (2005) reported that this technique used for detection of atrazine and dicamba herbicides from water samples. The procedure was based on oxidation of organophosphorus pesticides with slight excess of N-bromosuccinimide. The unconsumed N-bromosuccinimide was then reacted with rhodamine B which was followed by spectrophotometric estimation of decrease in color at 550 nm. The sensitivity of the methods was up to μg/g.

Even with limited success in these methods, some drawbacks were evident. They were 1) extensive sample preparation, 2) relatively slow and 3) could not be used for real time estimation. Hence these days' spectrophotometric methods are used only for detection of limited number of pesticides. Sometimes they are coupled with other systems as terminal detection devices to detect pesticides.

2.2.3. Electroanalytical Techniques

Electroanalytical techniques have gained importance for analysis of environmental samples. Their main advantages are simplicity in operation, sensitivity, selectivity, portability and so on. Commonly used electroanalytical techniques are: potentiometry, conductometry, voltammetry, amperometry.

Potentiometry

Potentiometry measures the potential of electrochemical cells. A potentiometric cell is composed of i) reference electrode ii) salt bridge iii) analyte solution and iv) indicator electrode.

Conductometry

It is based on the property of electrolyte solutions to dissociate into ions. It measures the change in electrical resistance of a solution. A conductometric cell consists of 1) two electrodes: Anode (positively charged) and cathode (negatively charged) 2) an electrolyte solution and 3) battery (current reading detection unit). The number of ions determines the amount of current generated which indicates the concentration of electrolytes.

Voltammetry

It measures the change in the current—potential characteristics of an electrochemical cell. This change is directly proportional to the concentration of the analyte. The current—potential relationship is dependent on the mass transfer rate. It is the rate at which the electroactive species generated due to oxidation reduction reactions reach the electrode.

Amperometry

Amperometry can be considered as a sub-class of voltammetry since both the procedures depend on the same principal. The only difference in voltammetry and amperometry is that in amperometry the potential applied across the cell is constant. It measures the current generated due to the oxidation-reduction reactions taking place in the analyte solutions.

2.2. Sensor

A sensor generally refers to a device that converts a physical measure into a signal that is read by an observer or by an instrument. Sensors can be used to measure or detect a vast variety of physical, chemical, and biological quantities, including chemicals, proteins, bacteria, gases, light intensity, motion, position, sound and many others, as shown in (Figure 4). Sensor measurements are converted by a transducer into a signal that represents the quantity of interest to an observer or to the external world (Chen, *et al*., 2012).

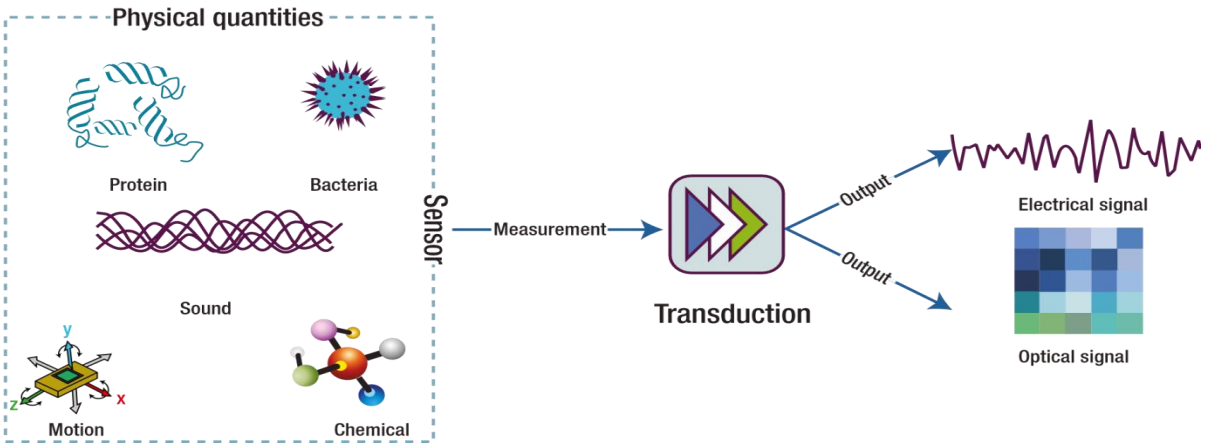

Figure 4. The sensing process

Sensors can be classified as physical and chemical sensors. A physical sensor is sensitive to physical responses such as pressure, temperature, etc., while a chemical sensor provides continuous response which relates to the quantity of a specific chemical species. A chemical sensor consists of a receptor element, which responds in a selective way, and a transducer, which converts the chemical information into an analytical signal. A good sensor has good

specificity and sensitivity, insensitivity to any other property likely to be encountered in its application, and does not influence the measured quantity (Mostafa 2010).

For any given quantity, there is usually more than one form of sensor that can be used to take a measurement. Each sensor type offers different levels of accuracy, sensitivity, specificity, or ability to operate in different environmental conditions.

2.2.1. Electrochemical Sensors

Electrochemical sensors are important subclasses of chemical sensors in which the electrode is used as the transduction element, and is highly qualified for meeting the size, cost, and power requirements of on-site environmental monitoring. Species can be determined quantitatively and qualitatively in solution. An electrochemical sensor is composed of a sensing or working electrode, a reference electrode, and, in many cases, a counter electrode. These electrodes are typically placed in contact with either a liquid or a solid electrolyte. In the low temperature range (<140 ℃), electrochemical sensors are used to monitor pH, conductivity, dissolved ions, and dissolved gases. For measurements at high temperatures (>500 ℃), such as the measurement of exhaust gases and molten metals, solid electrolyte sensors are used. Electrochemical sensors work on the principle of measuring an electrical parameter of the sample of interest. They can be categorized based on the measurement approach employed (Guth, *et al.,* 2009).

Electrochemical sensors can operate in potentiometric, sweep or pulse voltammetric techniques. Electrochemical sensors present a number of advantages, including low power consumption, high sensitivity, good accuracy, and resistance to surface-poisoning effects. Compared with other types of sensors, electrochemical sensors are most rapidly growing because of their remarkable sensitivity, experimental simplicity and low cost (Wang *et al.*, 2008). However, their sensitivity, selectivity, and stability are highly influenced by environmental conditions, particularly temperature. They are characterized by high sensitivity, good selectivity, wide linear range, minimal space and power requirements, and low-cost instrumentation. Electrochemical devices have been used in a wide range of applications for several decades for drugs, water contaminants, explosives, carcinogen monitoring,

development of (bio)sensors for the determination and control of pesticides, energy conversion and storage (Hanrahan *et al.*, 2004).

2.3. Nanomaterials for Sensor Application

Nanocomposites of metal-polymers or metal oxide-polymer composites are important classes of materials in the area of nanotechnology. Owing to small dimensional size, good conductivity and excellent catalytic activity of nanomaterials, composites of conducting polymers with metal nanoparticles can accelerate electron transfer rate, enhance conductivity of electrodes and have good biocompatibility in electronics, sensors and catalysis applications (Atta *et al.*, 2014).

2.3.1. Polyaniline (PANI)

Polyaniline (PANI) is one of the highly pursued conducting polymers in recent times owing to its excellent electrical and optical properties, better air and water stability and easy and cheap synthesis route. Due to these properties, polyaniline have been utilized for a variety of applications such as electrocatalysis, batteries, protection against corrosion and separation membranes. However, the utility of PANI limited in acidic media (pH < 3) and the neutral polymer is also insoluble in common solvents. (Genies *et al.*, 1990).

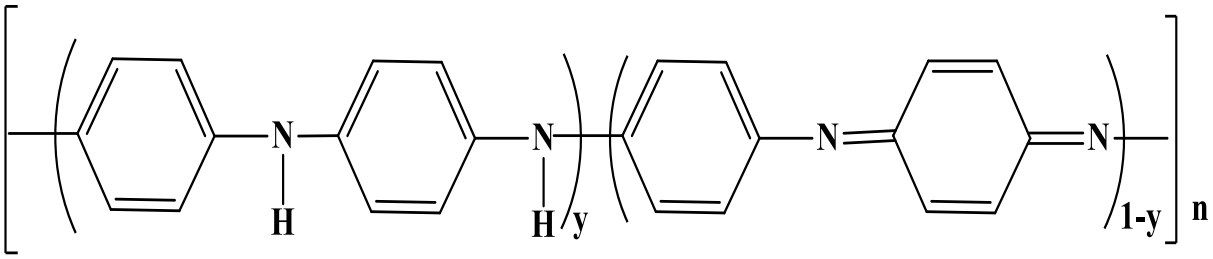

Figure 5. Polyaniline general formula

Polyaniline has three different oxidation states. The most important form of polyaninline, green protonated emeraldine and it is produced by the oxidative polymerization of aniline in aqueous acids. It's electrically conducting (conductivity s = 10^{-2} -10^{0} S/cm), due to the presence of cation radicals in its structure (Ryu *et al.*, 2002).

y=1 corresponds to leucoemeraldine, which is the fully reduced form of undoped PANI.
y=0.5 for emeraldine, which is the intermediate oxidation state of PANI.
y=0 for pernigraniline, which is the fully oxidized form of undoped PANI.

Based on the unique advantages of nanosized materials, a considerable amount of research has been carried out in developing methods for the production of nanoparticles and nanocomposites of electroactive polymers with noble metals or metal oxides. On this basis, electrochemical sensors based on metal nanoparticles–polyaniline composites such as, NiO/CuO/PANI (Ghanbari and Babaei 2016), graphene-PANI (Ruecha *et al.,* 2015) and graphene/PANI/polystyrene (Prompheta *et al.,* 2015) were developed.

2.3.2. Graphitic Carbon Nitride (g–C_3N_4)

Polymeric carbon nitride (CN) consists of earth-abundant carbon and nitrogen elements, generally has five phases. α–C_3N_4, β–C_3N_4, graphitic–C_3N_4, cubic–C_3N_4, and pseudo cubic–C_3N_4. Among all phases, graphitic carbon nitride (g–CN) was the most stable phase of CN at ambient conditions and it possesses a stacked 2-dimensional (2D) graphite-like planar structure, with N-heteroatoms substituted in the graphite framework containing p-conjugated systems maintaining a distance of 0.326 nm between two layers.

g- C_3N_4 is made up of only carbon and nitrogen and is stable in both acidic and basic media due to the presence of strong covalent bonds between the carbon and nitrogen atoms. In the molecular crystal, strong covalent bonds exist, but inside the molecular building blocks, there exists weak interactions, such as hydrogen bonding and van der Waals forces. It was found that in ideal g-CN architecture, an aromatic plane is constructed from triazine or tri-*s*-triazine units (Figure 6), and the aromatic planes in the structure are connected by weak van der Waals' forces and possesses high nitrogen content with excellent chemical and thermal stability (Groenewolt and Antonietti 2005).

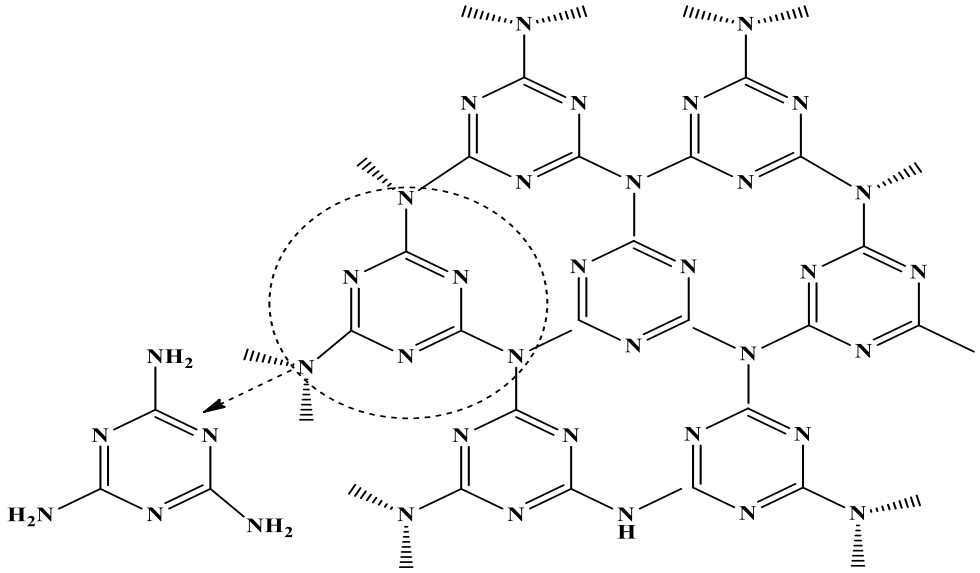

Figure 6. Tri-s-triazine-based connection patterns of g–C_3N_4 allotrope

Due to the different degree of condensation, the polymerized structure of g- C_3N_4 develops optimization in its packing, which makes the material behave as a multifunctional catalyst. The presence of a p-conjugated system modifies its bulk electronic structure and surface properties to allow it to exhibit: Electronic properties; Nucleophilic properties; the ability to form H-bonds; Photocatalytic activity. Through its special electronic properties, it can activate the Friedel–Craft reaction, Diels–Alder reactions and the timerisation of alkynes. Due to its nucleophillic properties, it helps in the activation of CO_2. Its ability to form H-bonds favours the trimerization of nitrides.

Similar to other delocalized conjugative P structure materials such as C_{60}, carbon nanotubes and graphene, it is proposed that g–C_3N_4 should also possess rapid charge separation and relatively slow charge recombination property in the electron transfer process (Wang and Zhang 2012). Different from the inorganic delocalized conjugative P materials (e.g., carbon nanotubes and graphene), g–C_3N_4 is a soft polymer so that it can easily coat on other compounds' surface. On the other hand, different from organic conjugative p materials such as polyaniline, g–C_3N_4 is often well-crystallized due to the nature of the lamellar structure, which facilitates the charge transfer. Its unique properties make wide applications in photovoltaic and photocatalytic fields, bio-imaging, sensing and catalysis (Tian *et al.*, 2013).

2.3.3. Cerium Dioxide (CeO_2)

Cerium oxides NPs have attracted great promise in nanotechnology due to their beneficial applications as catalysts, antioxidants, and biosensors in biological systems. In general, cerium can exist in two oxidation states: Ce^{3+} and Ce^{4+}. Therefore, cerium dioxide can have two different oxide forms, CeO_2 (Ce^{4+}) or Ce_2O_3 (Ce^{3+}), in bulk material. In nano scale, cerium oxide lattice has a cubic fluorite structure, while both Ce^{3+} and Ce^{4+} can coexist on its surface. Due to the presence of Ce^{3+}, charge deficiency is compensated by oxygen vacancy in the lattice, which provides oxygen defect in cerium oxide NPs. These oxygen defects are actually the sites of catalytic reactions. The concentration of oxygen defects increases as the particle size reduces; therefore, cerium oxides NPs have improved redox properties with respect to the bulk materials. Moreover, the presence of a mixed valance state plays an important role in scavenging reactive oxygen and nitrogen species.

Cerium dioxide nanostructure (nano CeO_2) is also one of the most promising semiconductor oxide material for bio fabrication due to their excellent properties, including good biocompatibility, vast surface-to-bulk ratio, high chemical stability, nontoxicity, excellent electronic conductivity and high isoelectric point (IEP). The high isoelectric point of CeO_2 (IEP $\approx$ 9.0) was suitable for the adsorption of a low IEP protein or enzyme via the electrostatic interactions (Xiao *et al.*, 2009).

Due to the above reasons and conversion of oxidation state, ceria is a key component in the so called three way catalysts commonly used as a base material of electrolytes and electrodes in solid oxide fuel cells and attracted much attention for the development of electrochemical sensor and biosensors in recent years (Ansari *et al.*, 2009).

2.3.4. Zinc Oxide (ZnO)

Zinc oxide crystallizes in two main forms, hexagonal wurtzite and cubic zinc blende. The wurtzite structure is most stable at environmental conditions and thus it is most common. By growing ZnO on substrates with cubic lattice structure, the zinc blende form can be stabilized. Zinc oxide (ZnO) is usually a semiconductor having wide band gap with an energy gap of 3.37 eV at normal room temperature. Due to their high catalytic activity and vast surface area, ZnO

nanostructures have a great benefit to be applied in a catalytic reaction process. Since Zinc Oxide presents different physical and chemical properties which depend on the morphology of nanostructures, not only various synthesis methods but also the physical and chemical properties of synthesized zinc oxide are to be investigated in terms of its morphology (Thirumavalavan *et al.,* 2013).

Zinc Oxide (ZnO) is analyzed to be a technologically remarkable material having a broad field of applications like semiconductor, gas sensor, piezoelectric sensor, electro luminescent material, magnetic material and actuator, ingredients of cosmetics (Hasanpoor *et al.*, 2016).

2.4. Various Synthesis Methods of Nanocomposites

There are different methods for the synthesis of the nanomaterials. Some of these are:

2.4.1. Impregnation Method

Impregnation methods used to seal porosity in electrical components, metal castings and powder metal parts. Metal-impregnated materials are typically prepared in a multi-step process: (1) oxide formation of precursor, (2) physical or chemical activation of the oxide product, (3) catalyst impregnation (using excess solution, incipient wetness, ion exchange, or chemical vapor deposition techniques), and (4) reduction or pyrolysis to form metal nanoparticles. The process is usually non-continuous and can require substantial time and energy. Each step requires heat, and at the activation, stage requires supplemental reagents to develop porosity. It requires a relatively low investment in equipment and cycle times are quicker. The wet impregnation method performs best for parts with large evenly distributed porosity such as powdered/sintered metal and does not require a pressure rated vessel. In addition impregnation method for the synthesis of mixed metal oxides has the following advantages: good homogeneity, low reaction temperature, fine and uniform particle size, easy scale-up, low cost, and time saving process. (Haber *et al*., 1995).

2.4.2. Co-precipitation Method

A facile and convenient method to prepare nanoparticles is chemical co-precipitation technique. Two or more soluble salts solutions are mixed in a definite ratio and co-precipitated with a base solution under inert atmosphere. Solutions of two or more water soluble salts of metals are dissolved in water, mixed and co-precipitated with alkali very slowly. At a simple level, precursors such as nitrates and carbonates can be used as starting materials instead of oxides: they decompose to the oxides on heating at relatively low temperatures, losing gaseous species, and leaving behind fine, more reactive powders (Faraji *et al*., 2010).

2.4.3. Hydrothermal Method

Hydrothermal synthesis can be defined as a method of synthesis of single crystals that depends on the solubility of minerals in hot water under high pressure. The crystal growth is performed in an apparatus consisting of a steel pressure vessel called autoclave, in which a nutrient is supplied along with water. A gradient of temperature is maintained at the opposite ends of the growth chamber so that the hotter end dissolves the nutrient and the cooler end causes seeds to take additional growth. The method has proved to be extremely efficient both in the search for new compounds with specific physical properties and in the systematic physicochemical investigation of intricate multicomponent systems at elevated temperatures and pressures. Possible advantages of the hydrothermal method over other types of crystal growth include the ability to create crystalline phases which are not stable at the melting point. Also, materials which have a high vapor pressure near their melting points can also be grown by the hydrothermal method. The method is also particularly suitable for the growth of large good-quality crystals while maintaining good control over their composition. Disadvantages of the method include the need of expensive autoclaves, and the impossibility of observing the crystal as it grows (O'Donoghue, 1983).

2.4.4. Sol-Gel Method

In Sol-gel technique discrete particles are integrated network precursor involved in chemical solution that mainly used for the fabrication of metal oxides hence it is a chemical technique. The precursor sol can be either deposited on the substrate to form a film or used to synthesize

powders. Sol-gel processing is a common chemical approach to produce high purity materials shaped as powders, thin film coatings, fibers, monoliths and self-supported bulk structures. The sol-gel process involves hydrolysis and condensation of the metal alkoxide followed by heat treatment at elevated temperatures which induce polymerization, producing a metal oxide network.

The sol-gel method has several advantages over other synthesis techniques such as purity, homogeneity, ease of preparation and ease of introducing dopants, composition and the ability to produce thin film coatings or porous powders. There are two possible routes for carrying out sol-gel synthesis, the non-alkoxide route and the alkoxide route. The non-alkoxide route uses inorganic salts as the starting material. This requires the removal of the inorganic anion to produce the required oxide. However, halides often remain in the final oxide material and are difficult to remove. The alkoxide route involves hydrolysis of metal alkoxide, followed by condensation. The hydrolysis/condensation reactions typically from a three dimensional polymeric structure, that, upon calcination will result metal oxide crystals depending on the calcination temperature (Keshmiri *et al.*, 2006).

2.5. Surface Characterization

Eventhough, electrochemical methods are powerful and sensitive in providing information about the kinetics of electron transfer and film porosity, they are limited in providing information about surface structure or elemental composition. Therefore, it needs other techniques in order characterize completely the surface of electrodes.

2.5.1. Scanning Electron Microscope (SEM)

SEM is a powerful microscopic method that uses beams of electrons rather than light to form an image of objects. It helps to characterize physical properties such as morphology, shape, size or size distribution of materials at the microscale and nanoscale. When the primary electron beam hits the specimen, atoms may be ionized by the forced emission of electrons which is referred to as secondary electrons. These secondary electrons are attracted to and detected by a positively charged detector and SEM is then translated into signals which are amplified and analysed before being translated into understandable images. The signals are

derived from electron-sample interaction and reveal information about the sample including external morphology (texture), chemical composition, crystalline structure and orientation of materials making up the sample (Rades *et al.,* 2014).

2.5.2. Fourier Transform Infrared Spectroscopy (FTIR)

FTIR is a rapid, nondestructive and time saving method that can detect the interaction between an infrared radiation and a sample that can be solid, liquid or gaseous. FTIR radiation encompasses a long range of wavelengths, which consists of other sub regions: near, middle and far infrared regions. However, most infrared spectroscopic measurements are performed in the mid- infrared region, which covers the spectral region between 400 cm^{-1} and 4000 cm^{-1}. It measures the frequencies at which the sample absorbs and also the intensities of these absorptions. Since, functional groups are responsible for the absorption of radiation at different frequencies; it is possible to identify the composition of a sample. The frequencies absorbed by the sample are helpful for the identification of the composition due to the fact that functional groups are responsible for the absorption of radiation at different frequencies. Individual absorption peaks can then be identified and assigned to individual chemical bonds which help for identification of individual compounds in complex systems qualitatively or quantitatively (Pradier *et al.,* 2005).

2.5.3. Ultraviolet-Visible Spectroscopy (UV-Vis)

Ultraviolet-visible spectroscopy (UV-Vis) is an analytical technique which involves the absorption of light by molecules in ultraviolet-visible region. The absorption in the visible range directly corresponds to the color of the chemicals involved. UV-Vis can be used to identify some chemical species and to determine the concentration of the solution based on the absorbance. This is because the wavelength at which a molecule absorbs light is a function of its electronic structure and the amount of UV-Vis light that is absorbed by a sample is related with the number (amount) of molecules. The amount light absorbed by a sample is proportional to the concentration of the absorbing species in accordance with the Beer-Lambert's law (Desai *et al.,* 2012).

$A = \varepsilon bc$

2.5.4. X-ray Diffraction (XRD)

X-ray diffraction is a conventional technique for determination of crystallographic structure and morphology. There is increase or decrease in intensity with the amount of constituent. This technique is used to establish the metallic nature of particles gives information on translational symmetry size and shape of the unit cell from peak positions and information on electron density inside the unit cell, namely where the atoms are located from peak intensities (Yelil Arasi *et al*., 2012). The average Crystallite size, D, can be calculated using the well-known Scherrer's equation:

$$D_{hkl} = (k*\lambda) / (\beta_{hkl}* Cos\theta_{hkl})$$

where D_{hkl} is the Crystallite size perpendicular to the normal line of (hkl) plane, k is a constant (0.94), β_{hkl} is the full width at half maximum of the (hkl) diffraction peak, θ_{hkl} is the Bragg angle of (hkl) peak and λ is the wavelength of X-ray (Goharshadi *et al.*, 2011).

2.6. Modified Electrodes

The concept of modified electrodes is certainly one of the exciting developments due to their wide range of applications, such as in electrocatalysis, corrosion protection, energy storage and electrochromic display (Chen *et al.*, 2009). In electroanalysis, the electrode itself can act as a reactant to pump (reduction) or withdraw (oxidation) electron in the reaction. Many compounds that are important biologically and environmentally show no response within a potential window at solid electrodes or for direct electrochemical detections usually require high potential. This can produce large background current, resulting in inferior detection limits. Also, passivation and deactivation of the electrode surface due to the adsorption of macromolecules or of reaction products, greatly affect the stability of the electrode response and reproducibility. Furthermore, coexisting components, which may be present in concentrations much larger than the analytes, may severely interfere within the determination of trace analytes. As a result, complicated sample pretreatments are often employed to eliminate or separate interfering components. These behaviors often can be controlled by manipulating the chemical nature of the electrode surface. In this case, the electrode surface

needs to be modified with an additional layer capable of interacting specifically with sample components.

Depending on the nature of interactions provided by additional layer, the response toward the target species is enhanced and/or the response of interfering species is attenuated. In either case an increase in the selectivity ratio analyte/interferent is observed. The underlying motivations of electrode surface modifications stem is the desire for improving electrocatalysis and freedom from surface fouling effects. Alternatively, electrodes can be modified to prevent undesirable reactions from competing kinetically with the desired electrode process. Conventional electrode materials such as metallic electrodes (Pt, Ag or Au) or carbon materials such as glassy carbon may serve as a substrate for modification. Metallic electrodes such as Au, Ag and Pt can be used as a base for modification because their surfaces provide reproducible results and clean surfaces can be produced and maintained in the laboratory environment (Malinauskas *et al.*, 2005).

The surface properties and reactivities of the electrodes can be controlled through surface modification, since the immobilization transfers the physicochemical properties of the modifier to the electrode surface. This process could impart a high degree of selectivity or sensitivity to the electrochemical transducers (Demirtas *et al.*, 2015). The modifier may act as a fast electron transfer mediator between the electrode and analyte species which is oxidized or reduced slowly or not at all at the bare electrode (Figure 7).

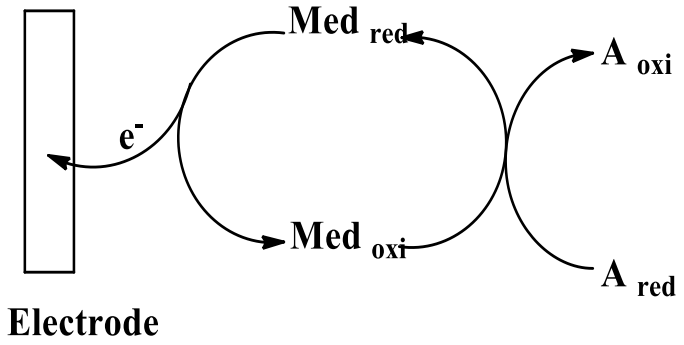

Figure 7. Electroctalytic reaction on chemically modified electrode

The transfer of electrons takes place between the electrode and mediator and not directly between the electrode and the analyte. In essence, then, the mediator can be considered to function simply as an electron shuttle between the electrode and the analyte. The net results of this electron shuttling are a lowering of the overvoltage to the formal potential of the mediator and increase in current density. There are various methods of modifying the surface of an electrode: physisorption, chemisorption, covalent attachment and electropolymerization.

2.7. Electroanalytical Techniques

Electroanalytical techniques have undergone many important developments in recent decades. They are routinely used for measurements in the laboratory, mostly for fundamental research in almost every chemical and biochemical research areas. They are not only used to study the nature of oxidation and reduction processes to unravel reaction mechanisms, but also used in studying the kinetics and thermodynamics of electron and ion transfer processes. Besides, it is apparent that electroanalytical techniques at varying levels of sensitivity are required to solve analytical problems. As a result, electroanalytical methods are widely used in specific studies and monitoring of industrial materials, biological samples and the environment. (Ronkainen *et al.,* 2010).

The choice of electroanalytical methods for analytical purpose depends upon the specific analyte, nature of the sample matrix, the parameter to be determined and the sensitivity and selectivity requirements. The techniques are characterized by instrumental simplicity, moderate cost and portability. Most electroanalytical techniques, such as cyclic voltammetry (CV), differential pulse voltammetry (DPV), square wave voltammetry (SWV) and stripping voltammetry are based on the concept of continuously changing the applied potentials at the electrode-solution interface and the resulting current is measured. (Hanrahan *et al.,* 2004)

2.7.1. Electrochemical Cells

The modern electroanalytical system for voltammetric measurements is usually composed of three components: a potentiostat, a personal computer and an electrochemical cell. Depending on the application, various cell designs and experimental assemblies are employed. The potentiostat consists of various components including electrometer circuits, various converters

and amplifiers, as well as microprocessors with internal memory. In order to perform electrochemical experiments quickly and to increase the sensitivity by discriminating capacitative currents, modern potentiostat in a digital system containing “staircase’’ modulated potential with ‘‘steps’’ can be utilized. The most frequent waveforms in modern potentiostats are linear or cyclic scan, differential pulse, and square wave. The choice of a particular instrument will be determined by the information (qualitative or quantitative) needed and the size of the electrodes. Depending on the type of techniques, the electrochemical cell can encompass a number of electrodes. For instance, potentiometry measurement requires two electrodes, while voltammetry three electrodes. Electroanalytical measurements with three electrodes systems are preferred over those involving two electrodes due to the reduction in uncompensated resistance. An electrochemical cell is considered to be a sample holder which consists of a solution of the analyte of interest, supporting electrolyte and the electrodes. The three electrodes are: working electrode, reference electrode and auxiliary or counter electrode.

Working Electrode (WE): It is an electronic conductor at which the reaction or transfer of electrons takes place. Solid or mercury-based electrodes are used as working electrodes in voltammetric techniques. In general, solid electrode materials have the advantage of being more mechanically stable, and they provide a larger anodic range than mercury based electrodes. The mercury electrode has high hydrogen overpotential and can be a choice for analytes reduced at higher cathodic potential.

Counter Electrode (CE): It is an electrode at which a counter reaction to that of the working electrode takes place. Pt wire, graphite, or thin pieces of gold are among the most frequently used as counter electrodes in voltammetric techniques. The purpose of the counter electrode is to preserve electroneutrality in the system, which is usually electrolysis of the supporting electrolyte or solvent and in order current flows without the need for using a large overpotential. Therefore, the area of counter electrode must be larger than the area of the working electrode in order to ensure the area of the electrode will not be a limiting factor in the kinetics of the electrochemical process under investigation (Thomas and Henze 2001).

Reference Electrode (RE): Reference electrode keeps the potential of an electrode constant regardless of the properties of the solution. The main criteria for an electrode to be classified

as a reference electrode are the tendency to provide a reversible half-reaction based on Nernstian behavior with a constant potential over time, and to be easy to assemble and maintain. Calomel electrode (Hg_2Cl_2(s)/Hg), and silver/silver chloride electrode (Ag/AgCl) are the most common reference electrodes (Farghaly *et al.*, 2014).

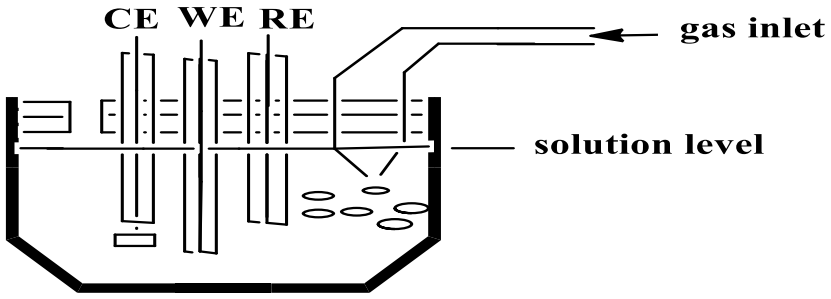

Figure 8. Schematic diagram of an electrochemical cell

Supporting Electrolytes: Supporting electrolytes are inert soluble substances added to the solution to avoid electrochemical reaction at the counter electrode during the course of electrochemical measurements. Since, the concentration of the supporting electrolyte is always much larger than (0.1 M – 1.0 M) that of the redox species unless ultramicroelectrodes are employed, it carries most of the ionic current and decrease the resistance of the solution by increasing the solution conductivity. Besides, it maintains a constant ionic strength and eliminates electromigration effects. The supporting electrolyte should be prepared from highly purified reagents, and should not be easily oxidized or reduced. Supporting electrolyte may be an inorganic salt, a mineral acid, a buffer or a chelating reagent (Stradiotto *et al.*, 2003).

2.8. Electrode Processes

Electrochemical reactions involve the transport of electroactive species to or from the electrode and the transfer of electrons across the interface. The net rate of the reaction and the measured current may be limited by either mass transport of the reactant or the rate of electron transfer. There are three ways in which material may be transported to the electrode surface: diffusion, migration and convection.

Diffusion is the spontaneous movement of electroactive species under the influence of concentration gradient, from regions of high concentration to regions of lower ones, aimed at

minimizing concentration differences. Concentration gradients between the vicinity of the electrode and the bulk solution arise as the analyte is consumed and the product is formed at the electrode.

Convection is the transport of the electroactive species to the electrode as a result of an imbalance forces on the solution. The driving force for convection is due to stirring the solution, rotating and vibrating the electrodes, or even simply expanding its volume (which is a movement of its surface against the solution) like dropping mercury electrode.

Migration is the movement of charged particles under the influence of an electric field generated by the electrode toward every ion having opposite charge. In addition, it is also due to the contemporary repulsion force of every ion having the same charge as the electrode.

2.9. Techniques and Instrumentation in Electrochemical Sensing

2.9.1. Cyclic Voltammetry (CV)

Cyclic voltammetry may provide the information of the thermodynamics of redox processes, adsorption processes and the kinetics of electron transfer reactions. It is the most widely used measuring technique in electrochemical analysis. In a typical cyclic voltammetry, the impulse potential is ramped linearly versus time and a pair of well-defined redox peaks is observed. Single or multiple cycles can be performed depending on the requirements of specific analysis. During cyclic voltammetric scanning, analytes will carry out certain electron communication with the electrode under various potentials and the currents may be proportional to the concentration of the analytes. The values of peak potentials and peak currents also provide the basis for classifying redox systems as reversible, irreversible or quasi-reversible systems (Leandro *et al.*, 2009).

Figure (9), Shows a series of cyclic voltammograms of $K_4Fe(CN)_6/K_3Fe(CN)_6$ solution obtained at an Au/cysteamine/AuNPs electrode with the treatment by AuNPs growth solution containing different amount of H_2O_2 (0, 0.1, 1, 10, 100, 1,000 μM H_2O_2). The peak currents are inversely proportional to the concentration of H_2O_2, demonstrating cyclic voltammetry a fine quantitative analytical method (Zhou *et al.*, 2006).

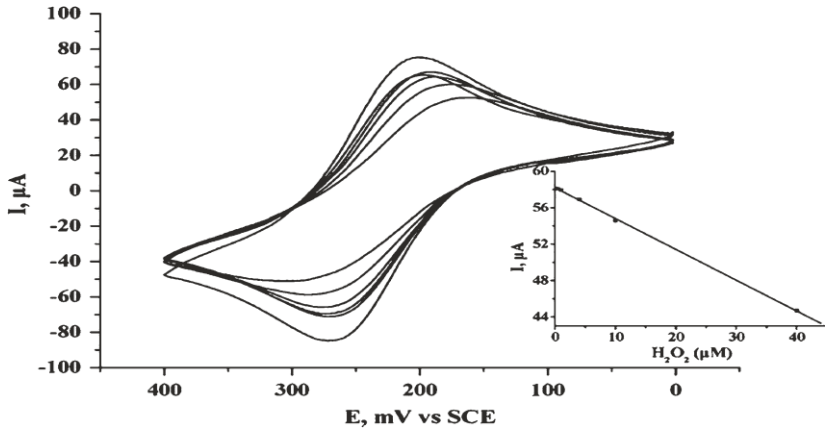

Figure 9. Cyclic voltammogram of $K_4Fe(CN)_6/K_3Fe(CN)_6$ solution obtained at Au/Cysteamine /AuNPs electrodes

2.9.2. Differential Pulse Voltammeter (DPV)

DPV is a derivative of linear sweep voltammetry and staircase voltammetry, which is extremely useful to detect trace levels of organic and inorganic analytes. In this technique, there are a series of regular voltage pulses superimposed on the potential linear sweep or stair steps. Just before each potential change and late in the pulse life, the currents are recorded. The current difference is then plotted against the applied potential. In the differential pulse voltammogram, the height of the current peak can be directly proportional to the concentration of corresponding analytes. The peak potential varies with different analytes, which can also be used to distinguish the detected species. DPV can not only help improve the sensitivity of the detection and the resolution of the voltammogram, but also provide information about the chemical form of the analytes, such as oxidation and complexation status, which is very important for an analysis (Li and Miao 2012).

2.9.3. Electrochemical Impedance Spectroscopy (EIS)

Impedance is a combination of resistors, capacitors, or inductors. EIS uses small amplitude perturbing sinusoidal voltage signal to an electrochemical cell and the resulting current response is measured. This small imposed perturbation can be an applied potential or applied current. Charge transfer resistance, Rct is the resistance associated with the charge transfer mechanisms for electrode reactions. It controls the electron transfer kinetics of a substance at

the electrode interface. The semicircle portion at higher frequencies in the Nyquist plot corresponds to the charge transfer resistance (Rct) at the electrode surface. Its value depends on the kind of the reaction, temperature, concentration of the reactants and the potential (Shamsipur *et al.*, 2015).

It has many advantages over the other electrochemical techniques. Since it applies a small amplitude AC signal, it is a non-destructive method for evaluating a wide range of materials, including coatings, anodized films and corrosion inhibitors. It can also be provide detail information of systems under examination; parameters such as corrosion rate, electrochemical mechanisms and reaction kinetics, detection of localized corrosion, can all be determined from these data. The response to the applied perturbation (potential or current) which is generally sinusoidal can differ in phase and amplitude from the applied signal (Hamdy *et al.*, 2006).

3. METHODOLOGY

3.1. Experimental Sites

Synthesis of nanosized PANI/ZnO, PANI/g–C_3N_4/ZnO, PANI/ZnO/CeO_2, and PANI/g–C_3N_4/ZnO/CeO_2 and with their respective modified glass carbon electrode, CV, EIS, DPV characterization and UV-Vis characterization were conducted at Chemistry department research laboratory, Haramaya University. FTIR characterization was done in Addis Ababa University Department of Chemistry Laboratory. XRD, SEM, TGA and BET characterizations were conducted in CSIC Madrid, Spain.

3.2. Instruments and Apparatus

CV, DPV and EIS experiments were performed using Bas100B Electrochemical Bioanalyzer in three electrode cell arrangement. The working electrode was glassy carbon (GC), platinum wire and silver/silver chloride (Ag/AgCl) were used as a counter and a reference electrode. UV–visible spectra of each nanomaterial were measured using (3 cm by 3 cm) quartz cuvette cell using a UV–Vis spectrophotometer (SANYO, SP65). FTIR spectra were reordered by using SHIMADZU (1730, Japan) spectrometer. XRD spectra were recorded by using X ’Pert Pro P analytical spectrophotometer. BET analysis was done by using Micrometrics ASAP2420. Thermogravimetric analysis (TGA) was performed on a Thermogravimetric analyzer PerkinElmer TGA7 and SEM characterization was done by using a Hitachi TM1000.

3.3. Chemicals and Reagents

Zinc acetate dihydrate (Germany, 98%), Cerium nitrate hexahydrate (India, 99%), Urea (India 98%), Aniline (Indian, 99%), Malathion (55%), Sodium dihydrogen phosphate (England, 98%), Disodium hydrogen phosphate (England, 98%), Oxalic acid (Switzerland, 99%), Ammonium persulphate (Germany, 98%), Potassium nitrate (99%), Potassium chloride (99%), Hydrochloric acid (England, 37%), Sodium hydroxide (England, 99%), Sulfuric acid (India, 98%), Nitric acid (69%), Methanol (98%), Ethanol (99.7%), Nitrogen gas (99.9%), Potassium ferricyanide (95%) and Alumina powders (1, 0.3 and 0.05 μm).

3.4. Procedures for the Synthesis of Nanomaterials

3.4.1. Synthesis of PANI/ZnO Nanocomposite

0.01 mol of $Zn(OAc)_2.2H_2O$ was dissolved in 50 mL distilled water and ethanol mixture (ratio 1:1) under stirring to form a transparent solution (solution A). Further solution B was obtained by dissolving 0.01 mol of oxalic acid in 50 mL distilled water and ethanol mixture (ratio 1:1). The oxalic acid solution (solution B) was added drop wise to the precursor solution (solution A) till slurry was formed. The slurry was further stirred for 5 hr. Then, the obtained precipitates were washed with distilled water and ethanol, and finally dried in an oven at 60 ℃. The dried product was calcined at 500 ℃ for 4 hr to get ZnO nanoparticle (Lamba *et al*., 2014). Before supporting the nanomaterials aniline was distilled. 0.81 g of ZnO powder was added in to 20 mL aqueous solution of 0.01 mol aniline monomer and 0.01 mol HCl. The 0.01 mol APS was dissolved in 15 mL distilled water and added drop wise to the mixture of ZnO and aniline with stirring in an ice bath. Polymerization proceeded for 5.5 hr. The composite of PANI modified ZnO was obtained as a precipitate.

3.4.2. Synthesis of PANI/CeO_2/ZnO Nanocomposite

0.01 mol of $Zn(OAc)_2.2H_2O$ and 0.00031 mol of $Ce(NO_3)_3.6H_2O$ were dissolved in 50 mL distilled water and ethanol mixture (ratio 1:1) under stirring to form a transparent solution (solution A). Further solution B was obtained by dissolving 0.01 mol of oxalic acid in 50 mL distilled water and ethanol mixture (ratio 1:1). The oxalic acid solution (solution B) was added drop wise to the precursor solution (solution A) till slurry was formed. The slurry was further stirred for 5 hr. Then, the obtained precipitates was washed with distilled water and ethanol, and finally dried in an oven at 60 ℃. The dried product was calcined at 500 ℃ for 4 hr to get ZnO/CeO_2 nanocomposite (Lamba *et al*., 2014). 2.53 g of ZnO/CeO_2 powder was added in to 20 mL aqueous solution of 0.01 mol aniline monomer and 0.01 mol HCl. The 0.01 mol APS was dissolved in 15 mL distilled water and added drop wise to the mixture of ZnO/CeO_2 and aniline with stirring in an ice bath. Polymerization proceeded for 5.5 hr. The composite of PANI modified ZnO/CeO_2 was obtained as a precipitate.

3.4.3. Synthesis of PANI/g–C_3N_4/ZnO Nanocomposite

0.25 mol of urea were heated to 550 ℃ with a heating rate of 2.5 ℃ /min and held 3 hr in a static air. The resultant agglomerates were grounded into fine powder. After that, the as prepared bulk g–C_3N_4 was further heated in an open ceramic container at 500 ℃ for 2 hr with a heating rate of 2 ℃/min. The resultant yellow product was collected and grounded to powder. (Jia *et al.,* 2016). 0.01 mol of zinc acetate dihydrate was dissolved in 2 mL deionized water, after which 0.15 g of g–C_3N_4 was added. The resulting mixture was allowed to set at room temperature for 4 hr. The water in the solution was then evaporated at 60 ℃. After drying at 80 ℃ for 12 hr, the sample was calcined at 300 ℃ for 2 hr to obtain the final ZnO/g–C_3N_4 (He *et al*., 2015). 0.913 g of ZnO/g–C_3N_4 powder was added in to 20 mL aqueous solution of 0.01 mol aniline monomer and 0.01 mol HCl. The 0.01 mol APS was dissolved in 15 mL distilled water and added drop wise to the mixture of ZnO/g–C_3N_4 and aniline with stirring in an ice bath. Polymerization proceeded for 5.5 hr. The composite of PANI modified ZnO/g–C_3N_4 was obtained as a precipitate.

3.4.4. Synthesis of PANI/g–C_3N_4/ZnO/CeO_2 Nanocomposite

0.02 g of nanosized CeO_2 powder was completely dispersed in ethanol by ultrasonication for 10 min and then 0.98 g of g–C_3N_4 was added into the above solution. Next, the mixture was stirred and dispersed by ultrasonication for 20 min, and the product was dried at 60 ℃ for 2 hr. Finally the g–C_3N_4/CeO_2 product was collected and calcined in the muffle furnance at 300 ℃ for 1 hr. Typically 1.0 g as-prepared bulk g–C_3N_4/CeO_2 was dispersed in the mixture of concentrated H_2SO_4 20 mL and HNO_3 20 mL for about 2 hr at room temperature. Then the resulting product was separated by centrifugation for 5 min at about 5000 rpm. So that composite nanosheet was obtained (Yuan *et al.,* 2017). Finally the sample was washed with distilled water and ethanol to remove the residual acid and dried at 80 ℃ for 12 hr.

Finally 0.246 g as prepared g–C_3N_4/CeO_2 composite nanosheets was dispersed in 40 mL methanol and sonicated for 1 hr. Then, 0.243 g of ZnO powder was added in to the above solution and stirred in a fume hood for 24 hr. After volatilization of methanol powder was obtained by drying at 100 ℃ in the air. 0.913 g of g–C_3N_4/ZnO/CeO_2 powder was added in to

20 mL aqueous solution of 0.01 mol aniline monomer and 0.01 mol HCl. The 0.01 mol APS was dissolved in 15 mL distilled water and added drop wise to the mixture of g–C_3N_4/ZnO/CeO_2 and aniline with stirring in an ice bath. Polymerization proceeded for 5.5 hr. The composite of PANI modified g–C_3N_4/ZnO/CeO_2 was obtained as a precipitate.

3.5. Preparation of Buffers

The 0.1 M phosphate buffers were prepared by weighing approximately 0.8 g of $NaH_2PO_4.2H_2O$ and 6.518 g of Na_2HPO_4 then dissolving into a 500 mL volumetric flask. It was adjusted with 0.1 M HCl and 0.1 M NaOH to the desired pH (4 to 8) and the final volume with deionized water. All buffer solutions were stored in the fridge at 4 ℃. Determining the pH with high peak was carried out by characterizing modified electrode in each pH range (4 to 8) (Bisetty *et al*., 2011).

3.6. Modification of GCE

Before drop coating as synthesized nanomaterials on bare GCE the electrode was polished with 1.0, 0.3 and 0.05 μm alumina powder, rinsed with distilled water followed by ultrasonication with and deionised water and ethanol respectively, and dried at room temperature. 3 mg of each PANI/ZnO, PANI/ZnO/CeO_2, PANI/g–C_3N_4/ZnO, and PANI/g–C_3N_4/ZnO/CeO_2 dissolved in 3 mL of ethanol and ultrasoncated. Then approximately 15 μL of the above suspensions were then drop-coated onto the surface of a bare glassy carbon electrode and dried at room temperature to obtain PANI/ZnO/GCE PANI/ZnO/CeO_2/GCE PANI/g–C_3N_4/ZnO/GCE, and PANI/g–C_3N_4/ZnO/CeO_2/GCE electrode respectively. The characterizations of each chemically modified electrode were done with potential range of −300 to 700 mV.

3.7. Preparation and Determination of Real Sample

Khat leaf sample was collected purposively from farm land, Awodey woreda, Eastern Hararge zone for malathion extraction. 5 g of khat was torn into very small pieces and grinded using pistol and mortar. The powder was added in to a flask that contains 20 mL of methanol and sonicated for 15 min. The mixture is filtered through a Buchner funnel to separate the liquid

from the solid plant material and the liquid part was diluted by adding 5 mL of deionized water.

3.8. Important Properties of PANI/g–C_3N_4/ZnO/CeO_2 Modified Electrode Study

All important properties of the modified electrode were investigated by using differential pulse voltammeter in 0.1 M phosphate buffer and 2.0 mM potassium ferrocyanide in potassium chloride solution at pH of 7.0. Stability and reproducibility of the modified electrode sensor was evaluated by measuring its current response to 4×10^{-8} M malathion within a 15 day period. The recovery experiment was evaluated by using 4×10^{-8}, 6×10^{-8}, and 8×10^{-8} M standard malathion solution. Interference analysis was performed, and the peak current compared with that of 4×10^{-8} M malathion.

3.9. Characterization of Nanocomposites

3.9.1. Structural Characterizations

The FTIR spectrum of the as-synthesized nanocomposites was determined using the KBr disc method. The IR absorption pattern was recorded between 400 and 4000 cm^{-1} using SHIMADZU (1730, Japan) spectrometer. Powder X-ray diffraction pattern was recorded with X'Pert Pro PANalytical with CuKa radiation (l = 1.5405 Å). The data were registered with 2θ steps of 0.02^o and accumulation times of 20 s. N_2 adsorption isotherms were measured at -196 ℃ (77 K) on Micromeritics ASAP2420 and the micropore surface area and volumes were calculated by the Brunauer–Emmett–Teller (BET) method. UV-Vis absorption were measured using SANYO, SP65 spectrophotometer by scanning over 200 – 800 nm wavelength. Thermogravimetric analysis (TGA) was performed on a Thermogravimetric analyzer PerkinElmer TGA7. Samples were heated at a rate of 20 ℃/min to a maximum temperature of 700 ℃ in a flowing atmosphere of oxygen. The morphology and particle size distribution of the solids were determined by scanning electron microscopy (SEM) using a Hitachi TM1000.

3.9.2. Electrochemical Characterizations

The electrochemical characterizations of chemically prepared nano-structures were characterized using CV, EIS and DPV. The working status of 100BASS electrochemical bioanalyzer and reference electrode was calibrated with respect to the potassium ferrocyanide in potassium chloride solution after polishing of GCE with alumina powder (1, 0.3 and 0.05 μm).

The CV behavior of each nanocomposite on the surface of GCE was studied in 0.1 M PBS + 2 mM $K_4[Fe(CN)_6]$ + 0.1 M KCl by ranging potential window from -300 to 700 mV at different scan rates. EIS study of as-synthesized nanocomposites were performed at 5 mV amplitude at different formal potential by ranging frequency from 0.1 to 10 KHz by using 0.1 M PBS + 2 mM potassium ferrocyanide in 0.1 M potassium chloride solution. The DPV experiment was carried out using PANI/g–C_3N_4/ZnO/CeO_2/GCE in pH 7.0 PBS + 2 mM potassium ferrocyanide in 0.1 M potassium chloride solution containing 2.0×10^{-8} to 14.0×10^{-8} M malathion solution. All the electrochemical experiments were carried out at room temperature and deionized water was used throughout.

3.10. Optimization for Malathion Sensing

3.10.1. pH Optimization

The effect of pH on malathion oxidation was investigated in the pH range of 4 to 8. The pH was maintained each time by using 0.1 M HCl and 0.1 M NaOH measured using a pH meter under constant scan rate.

3.10.2. Scan Rate Optimization

To investigate how scan rate influence the electrochemical response of PANI/g–C_3N_4/ZnO/CeO_2/GCE in malathion solution, CVs were operated under different scan rates from 10 to 100 mVs^{-1} with an interval of 10 mVs^{-1} in 0.1 M PBS + 2 mM potassium ferrocyanide in 0.1 M potassium chloride + 2.0×10^{-8} M malathion at pH 7.0.

4. RESULTS AND DISCUSSION

4.1. X-ray Diffractions Analysis (XRD)

The XRD pattern of PANI/ZnO, PANI/ZnO/CeO_2, PANI/g–C_3N_4/ZnO, and PANI/g–C_3N_4/ZnO/CeO_2 on the GCE substrate is illustrated in (Figure 10). The broad peak at 2θ value at 10 to 30 is due to the amorphous nature of polyaniline (Ghanbari and Babaei 2016: Chaudhari and Kelkar 1996). The peaks located at 31.9, 34.5, 36.4, 47.7, 56.7, 62.9,and 68.1 in all nanocomposites (PANI/ZnO, PANI/ZnO/CeO_2, PANI/g–C_3N_4/ZnO, and PANI/g–C_3N_4/ZnO/CeO_2) related to the crystal plane of (100), (002), (101), (102), (110), (103), and (112) respectively [96–210–7060] (Yuan *et al.,* 2017). The diffraction peaks can be well indexed to the hexagonal wurtzite ZnO.

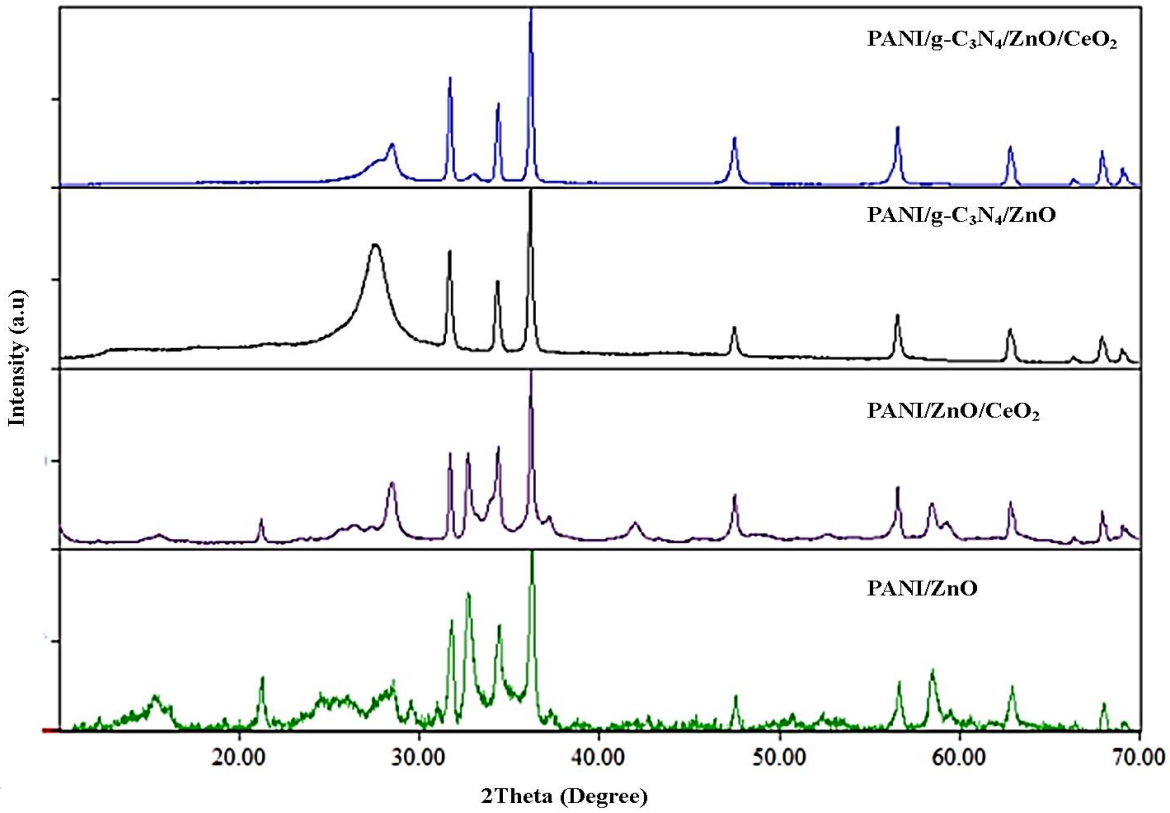

Figure 10. XRD patterns of PANI/ZnO, PANI/ZnO/CeO_2, PANI/g–C_3N_4/ZnO and PANI/g–C_3N_4/ZnO/CeO_2

Peaks at 28.8 in (PANI/ZnO/CeO_2 and which is overlapped with C_3N_4 at PANI/g–C_3N_4/ZnO/CeO_2) and peak at 56.6 which is overlapped with ZnO in PANI/ZnO/CeO_2 and PANI/g–C_3N_4/ZnO/CeO_2 corresponds to (111) and (311) plane the CeO_2 crystal phase [96–152– 4574] (Lamba *et al.,* 2015). The diffraction peaks indexed to the cubic CeO_2.

The characteristic interlayer stacking (002) peak of the aromatic system of g–C_3N_4 in PANI/g–C_3N_4/ZnO composites shifts slightly to a higher angle, from 2θ of 27.65 to 28.60 of PANI/g–C_3N_4/ZnO/CeO_2 [96–711–5196] which is due to the crystal lattice distortion in g–C_3N_4 owing to the relatively strong interaction between the CeO_2 and g–C_3N_4 caused by incorporation of CeO_2 with g–C_3N_4 (Yuan *et al.,* 2017).

The average Crystallite size, D, can be calculated using the well-known Scherrer's equation:

$$D_{hkl} = (K \times \lambda) / (\beta_{hkl} \times Cos\theta_{hkl})$$

Where D is the Crystallite size perpendicular to the normal line of (hkl) plane, K is a constant (0.94), β is the full width at half maximum of the most intense peak (in radians), and θ is the Bragg angle of the most intense peak (hkl) and λ is the wavelength of X-ray. From this result PANI/g-C_3N_4/ZnO/CeO_2 nanocomposite have small particle size so making it amenable to sensor application.

Table 1. Crystal size of the synthesized nanocomposites from XRD patterns

Sample	D_{hkl}(nm)
PANI/ZnO	65.28
PANI/ZnO/CeO_2	43.52
PANI/g-C_3N_4/ZnO	32.61
PANI/g-C_3N_4/ZnO/CeO_2	21.86

4.2. FTIR Spectroscopy

Figure (11), Shows the typical FTIR spectrum of the PANI/ZnO, PANI/ZnO/CeO_2, PANI/g–C_3N_4/ZnO, and PANI/g–C_3N_4/ZnO/CeO_2 nanostructures which are done in the range of 400 to 3600 cm^{-1} wavenumber, which identify the chemical bonds as well as functional groups in the compound.

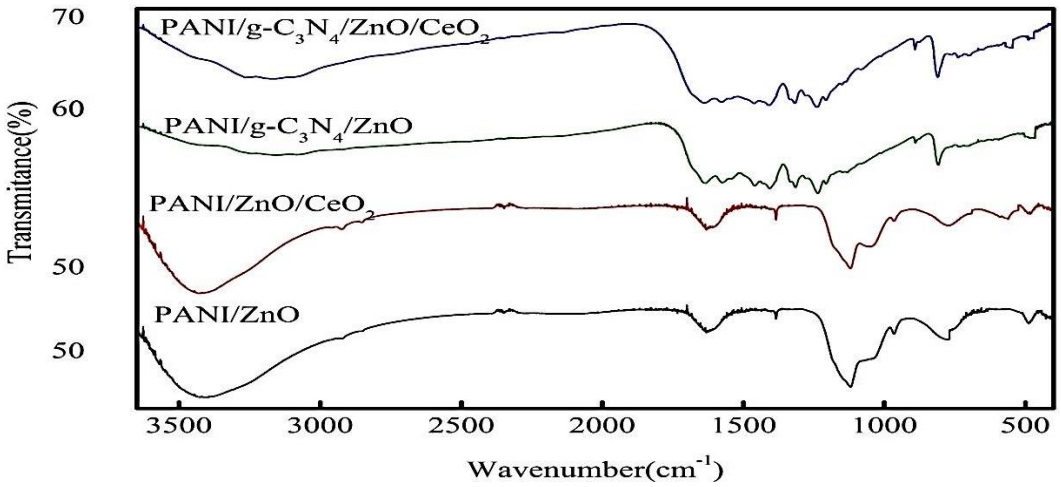

Figure 11. FT-IR spectra of the nanocomposites

The large broad band at 3415 cm^{-1} (PANI/ZnO and PANI/ZnO/CeO_2) is ascribed to the O–H stretching vibration in OH^- groups. The broad band at around 3100 – 3400 cm^{-1} (PANI/g–C_3N_4/ZnO and PANI/g–C_3N_4/ZnO/CeO_2) is assigned to the NH moieties, as well as to the adsorbed hydroxyl groups of H_2O. The peaks around 488 cm^{-1} in all nanocomposite is attributed to the Zn–O stretching vibration (Musić *et al.,* 2002). An absorption band around at 554 cm^{-1} (PANI/ZnO/CeO_2 and PANI/g–C_3N_4/ZnO/CeO_2) is the characteristic peak for the Ce–O stretching vibration (Khan *et al.,* 2011). The peak at 805 cm^{-1}, (PANI/g–C_3N_4/ZnO and PANI/g–C_3N_4/ZnO/CeO_2) assigned to the triazine group of g–C_3N_4, was observed in composite samples containing the moiety, indicating intense interaction between ZnO and g–C_3N_4 (Jo *et al.,* 2015).

In the FT-IR spectrum of g–C_3N_4, (PANI/g–C_3N_4/ZnO and PANI/g–C_3N_4/ZnO/CeO_2) several strong bands in the 1200 – 1650 cm^{-1} region were found, which correspond to typical stretching modes of CN heterocycles (Li *et al.,* 2014). The peaks at 1235 and 1318 cm^{-1} were assigned to CN stretching vibrations while those at 1406, 1450, 1560 cm^{-1} are likely due to heptazine-derived repeating units (Xu *et al.,* 2012). The peaks at 1,126 cm^{-1} (PANI/ZnO and PANI/ZnO/CeO_2) are due to the in-plane bending vibration mode of C–H, which is associated with high electrical conductivity and high degree of electron delocalization of polyaniline (Hasoon and Hadi 2018) and peak at 804 cm^{-1} is due to C–H para-substituted aromatic ring (Ai *et al*., 2010). The peak around 1600 cm^{-1} may due to deformation vibration of H_2O molecule.

4.3. UV-Vis Spectroscopy

The optical absorption analyses of the samples were investigated by UV–Vis diffuse reflectance's spectroscopy over the wavelength range, 200 – 800 nm. As expected, a sharp fundamental absorption edge for PANI/ZnO rose at 400 nm, attributable to the 3.11 eV band gap and which is in agreement with Qin *et al*. (2017) of ZnO with band gap of 3.18. The main absorption edge of PANI/ZnO/CeO_2 occurred at 411 nm corresponding to a typical band-gap of 3.01 eV. Lamba *et al*. (2015) also reports, the band gap of ZnO/CeO_2 was 3.05 eV.

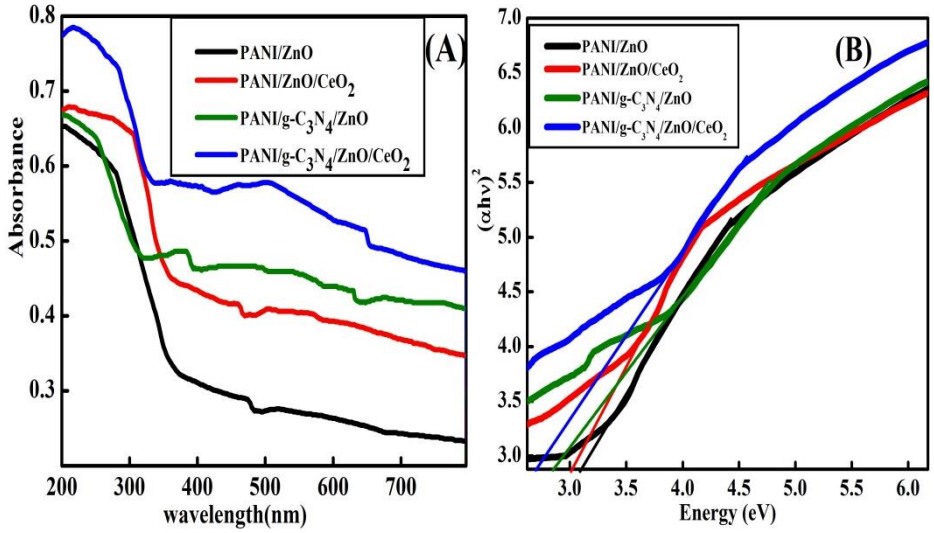

Figure 12. A) UV–Vis absorption spectra of the nanocomposites. B) plot of $(\alpha h\nu)^2$ versus energy ($h\nu$) for the band gap energy of the nanocomposites

The absorption edge of PANI/g–C_3N_4/ZnO occurs at 435 nm and corresponding to 2.85 eV which agrees well with the previous report. Qin *et al*. (2017) reported that g–C_3N_4/ZnO possesses a band gap of 2.9 eV. The UV–Vis spectrum of the prepared PANI/g–C_3N_4/ZnO/CeO_2 composite is at about 451 nm and the corresponding band gap is about 2.75 eV.

The above result showed that PANI/g–C_3N_4/ZnO and PANI/g–C_3N_4/ZnO/CeO_2 nanomaterials show extended absorbance to the visible region than PANI/ZnO and PANI/ZnO/CeO_2; this is due to the presence of g–C_3N_4. He *et al.* (2015) reported that pure g–C_3N_4 exhibits band gap of 2.63 eV.

The PANI/g–C_3N_4/ZnO/CeO_2 exhibited the smallest band gap, improving its conductivity. The shift of the absorption edge and the substantial decrease in the band gap may due to the interaction and synergism between g–C_3N_4, ZnO and CeO_2 within the PANI/g–C_3N_4/ZnO/CeO_2 nanocomposite. This may enhance the electrochemical properties of PANI/g–C_3N_4/ZnO/CeO_2. The energy difference between the two bands in PANI/g–C_3N_4/ZnO/CeO_2 is small. So that passage of an electrical current enhances the electrochemical property of PANI/g–C_3N_4/ZnO/CeO_2 as compared to PANI/ZnO, PANI/ZnO/CeO_2, and PANI/g–C_3N_4/ZnO.

4.4. Scanning Electron Microscopy

In order to investigate the morphology of the samples, SEM observation was carried out and Figure 13 shows typical SEM images of PANI/ZnO, PANI/ZnO/CeO_2, PANI/g–C_3N_4/ZnO and PANI/g–C_3N_4/ZnO/CeO_2. PANI/ZnO shows a snow-ball like spheres comprising nanorods of the binary composite.

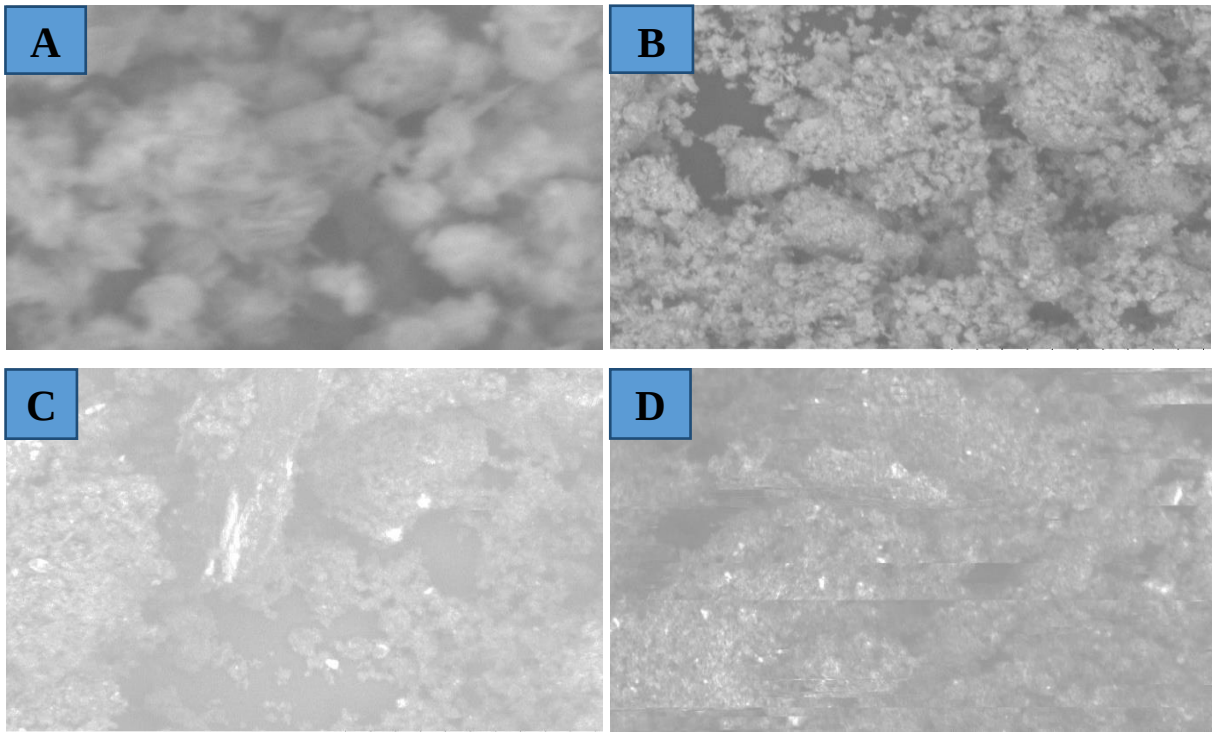

Figure 13. SEM pictures of A) PANI/ZnO, B) PANI/ZnO/CeO_2, C) PANI/g–C_3N_4/ZnO and D) PANI/g–C_3N_4/ZnO/CeO_2

Addition of CeO_2 as a component in the composite PANI/ZnO/CeO_2 showed aggregates of irregular nanoparticles with no distinct morphology. The introduction of CeO_2 appeared to restrain the growth of nanorods observed in the case of PANI/ZnO. Addition of g–C_3N_4 in both systems (PANI/ZnO and PANI/ZnO/CeO_2) resulted in aggregates of small particles of no defined morphology as well.

4.5. Surface Area Analysis

The nanocomposites redox reaction takes place mainly on the surface of the nanocomposites, and therefore the surface properties significantly influence the efficiency of redox activity. Specific surface area of the nanocomposites was evaluated by nitrogen adsorption–desorption. The corresponding values for PANI/ZnO, PANI/ZnO/CeO_2, PANI/g–C_3N_4/ZnO and PANI/g–C_3N_4/ZnO/CeO_2 composites were 7.8246, 8.5912, 10.1411 and 29.7780 m^2g^{-1}, respectively. The surface area of the PANI/g–C_3N_4/ZnO/CeO_2 composite significant increase compared to the other samples. This may due to synergistic effect between the nanoparticles which lead to the small size of nanocomposites.

Table 2. Crystallite size and BET surface area of the synthesized nanocomposites

Sample	Crystallite size D (nm)	BET surface area (m^2g^{-1})
PANI/ZnO	65.28	7.8246
PANI/ZnO/CeO_2	43.52	8.5912
PANI/g–C_3N_4/ZnO	32.61	10.1411
PANI/g–C_3N_4/ZnO/CeO_2	21.86	29.7780

From the XRD results, the nanocomposite materials exhibit smaller size that promotes high surface area which was confirmed by BET analysis. The results of BET specific surface area, and XRD crystal size are tabulated in Table 2.

4.5. Thermal Analysis

The thermal stability of the nanocomposites has been analyzed based on the DTA/TGA analysis of the samples (Figure 14). The temperature range between (25 ℃ – 700 ℃) was used. The total weight loss for the first two samples has been found to be 13% (PANI/ZnO) and 10% (PANI/ZnO/CeO_2). The first stage of weight loss of PANI/ZnO and PANI/ZnO/CeO_2

from 50 ℃ to 315 ℃ is mainly ascribed to the loss of the physically adsorbed water on the surface of composites and the removal of intermolecular H–bonded, while weight loss approximately from 315 ℃ to 405 ℃ mostly corresponds to the decomposition of organic ingredients (Hu and Zhou 2016). At high temperature i.e. 410 – 700 ℃, the weight loss was about 1.67% for PANI/ZnO and 0.71% for PANI/ZnO/CeO_2 only. This clearly indicated the thermal stability of the synthesized sample.

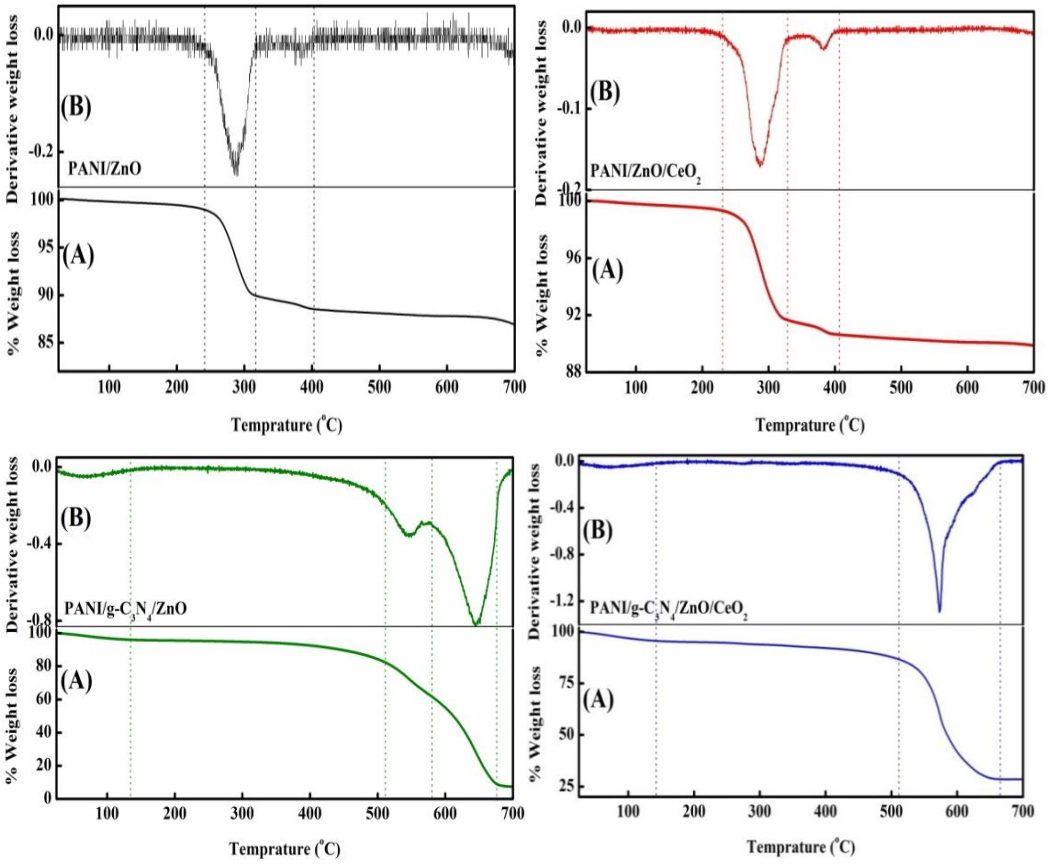

Figure 14. A) TGA and B) DTG curve of the nanocomposites

In the TGA curves of the PANI/g–C_3N_4/ZnO and PANI/g–C_3N_4/ZnO/CeO_2 total weight loss found to be 89% and 71% respectively. The first stage of weight loss occurs in the temperature range from 25 to 150 ℃ which correspond to the removal of water adsorbed by nanocomposites. The second weight loss occurs from 200 to 505 ℃ corresponds to the decomposition of the polymer PANI. The stability of nanocomposites greatly decreased from 550 – 675 ℃ due to the oxidation and decomposition of g–C_3N_4 in the PANI/g–C_3N_4/ZnO and PANI/g–C_3N_4/ZnO/CeO_2 nanocomposites (Jia *et al.*, 2016).

4.6. Electrochemical Properties of Chemically Modified Electrodes

Prior to modification, the glass carbon electrode (GCE) was successively polished with 1, 0.3 and 0.05 µm alumina slurry, and then was ultrasonically cleaned in water for 5 min. PANI/ZnO, PANI/ZnO/CeO_2, PANI/g–C_3N_4/ZnO, PANI/g–C_3N_4/ZnO/CeO_2 (2 mg) was dissolved in 2 mL of ethanol and shacked to form a suspension. 5 µL of the prepared materials suspension was drop coated on cleaned GCE and dried at room temperature to obtain PANI/ZnO/GCE, PANI/ZnO/CeO_2/GCE, PANI/g–C_3N_4/ZnO/GCE and PANI/g–C_3N_4/ZnO/CeO_2/GCE modified electrode.

4.6.1. Cyclic Voltammetry Characterization

The electrochemical behaviors of the electrodes were investigated using cyclic voltammetry (CV) and electrochemical impedance spectroscopy (EIS) in 0.1 M phosphate buffer and 2.0 mM potassium ferrocyanide in potassium chloride solution. Figure 15, represents the CV responses of PANI/ZnO, PANI/g–C_3N_4/ZnO, PANI/ZnO/CeO_2 and PANI/g–C_3N_4/ZnO/CeO_2 GC modified electrode in 0.1 M PBS + 2 mM $K_4[Fe(CN)_6]$ + 0.1 M KCl at pH 7.0 and 50 mVs^{-1} scan rate and potential window from −300 to 700 mV.

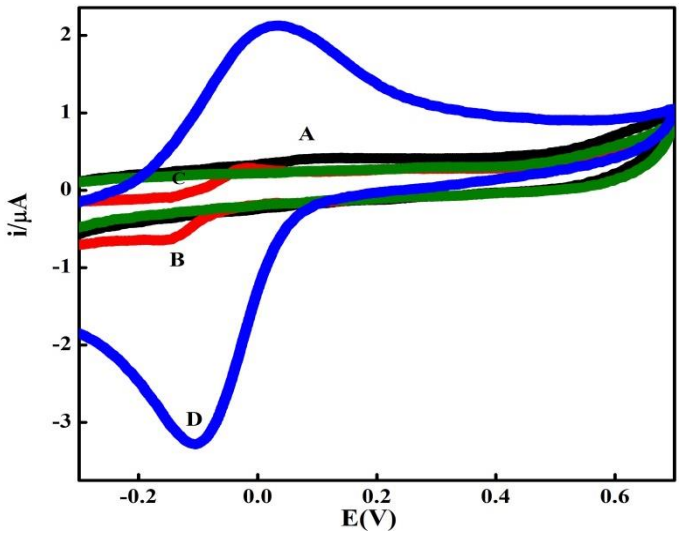

Figure 15. Cyclic voltammetry curves of A) PANI/ZnO, B) PANI/ZnO/CeO_2, C) PANI/g–C_3N_4/ZnO and D) PANI/g–C_3N_4/ZnO/CeO_2 at 50 mVs^{-1} scan rate

As observed from the above voltammogram there is no redox peaks on modified GCE in the case of PANI/ZnO and PANI/g–C_3N_4/ZnO but one oxidation and one reduction peak appeared for the electrodes modified by PANI/CeO_2/ZnO and PANI/g–C_3N_4/ZnO/CeO_2. CeO_2 NPs in the composite facilitates the electron transfer process and excellent conductibility. This allows easier electron flow between and even interface with the active sites of the nanocomposite and electrode surface.

Large peak current was recorded when the ternary system on electrode compared with that of the binary system. This may due to the presence of metal oxides (ZnO/CeO_2) anchored on the surface of g–C_3N_4 nanosheets and forms g–C_3N_4/ZnO/CeO_2 hybrid composite. So that g–C_3N_4/ZnO/CeO_2 hybrid composite accelerates the tunneling of electrons transport. Such results revealed that the existence of synergistic effect in the composite film, and the synergistic effect could facilitate the interfacial electron transfer (Zhang *et al.,* 2012).

Malathion oxidation was conducted in 0.1 M PBS in 0.1 M phosphate buffer and 2.0 mM potassium ferrocyanide in potassium chloride solution with 2×10^{-8} M as shown in (Figure 16) using the various modified GCE from −300 to 700 mV potential range at scan rate of 50 mVs^{-1}. As shown in the voltammograms no redox process occurred on PANI/ZnO/GCE and PANI/g–C_3N_4/ZnO/GCE in the presence of malathion (solid line), indicating that PANI/ZnO and PANI/g–C_3N_4/ZnO cannot undergo the redox reaction in the experimental potential ranges.

On the other hand, PANI/ZnO/CeO_2/GCE and PANI/g–C_3N_4/ZnO/CeO_2/GCE electrodes exhibit a pair of redox peaks. PANI/ZnO/CeO_2 exhibits with the anodic and cathodic peaks at approximately −20 and −149 mV, whereas in the case of PANI/g–C_3N_4/ZnO/CeO_2 electrode the peaks formed at + 39 and −108 mV, respectively. Therefore, the anodic and cathodic peaks at the PANI/ZnO/CeO_2 and PANI/g–C_3N_4/ZnO/CeO_2 modified electrode should be ascribed to the electron transfer process in the nanocomposite due to CeO_2 nanoparticle in the modified electrodes.

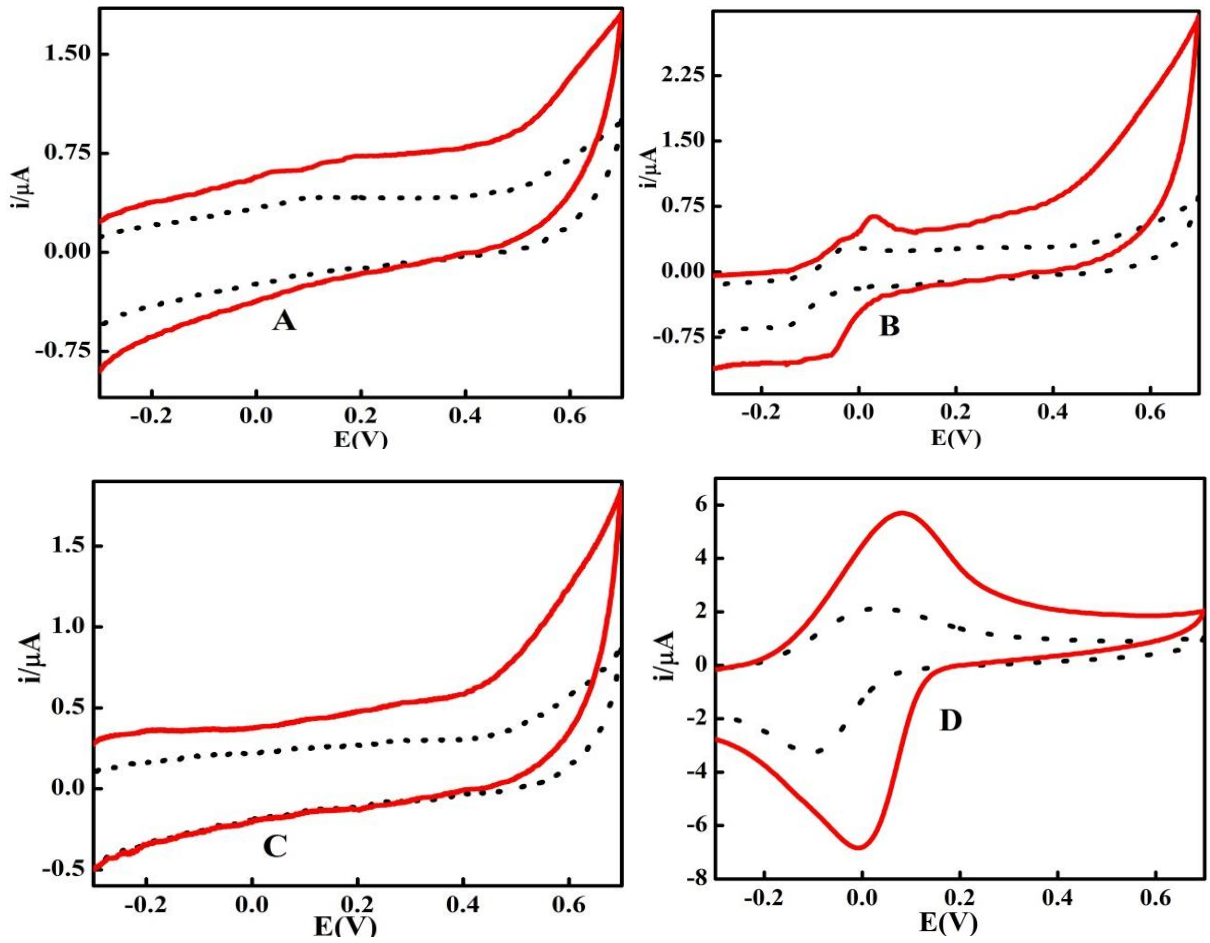

Figure 16. Cyclic voltammograms of A) PANI/ZnO B) PANI/ZnO/CeO_2 C) PANI/g–C_3N_4/ZnO and D) PANI/g–C_3N_4/ZnO/CeO_2 nanocomposites in the absence (dotted line) and presence (solid line) of 2.0×10^{-8} M malathion in 0.1 M PBS + 2 mM $K_4[Fe(CN)_6]$ + 0.1 M KCl. The scan rate is 50 mVs^{-1}.

Upon PANI/g–C_3N_4/ZnO/CeO_2 electrode, peak potential of the oxidation reaction shift to more positive positions with a concomitant increase in the peak currents than other electrodes. Upon PANI/g–C_3N_4/ZnO/CeO_2/GCE, oxidation peak at about 39 mV is observed (curve D Figure 16), which is 59 mV positively shifted compared with that of ZnO/CeO_2/GCE. This indicates the hybrid film exhibits catalytic response characteristic of PANI/g–C_3N_4/ZnO/CeO_2 nanocomposite.

4.6.2. Electrochemical Impedance Spectroscopy

Electrochemical impedance spectroscopy (EIS) was carried out to investigate the electrical behavior of the modified electrode surface. In EIS, the semicircle diameter of impedance spectroscopy equals the interfacial electron transfer resistance (Ret), which controls the electron transfer kinetics of the redox probe at the electrode surface. Figure 17 show that the EIS spectra of nanocomposite modified electrode. The semicircular diameter of the PANI/ZnO/GCE, PANI/ZnO/CeO_2/GCE, PANI/g–C_3N_4/ZnO/GCE and PANI/g–C_3N_4/ZnO/CeO_2/GCE decreases respectively. This finding indicates that the PANI/ZnO, PANI/ZnO/CeO_2, PANI/g–C_3N_4/ZnO electrode results a higher magnitude of charge transfer resistance than PANI/g–C_3N_4/ZnO/CeO_2. This suggesting PANI/g–C_3N_4/ZnO/CeO_2 electrode enhances electron transfer.

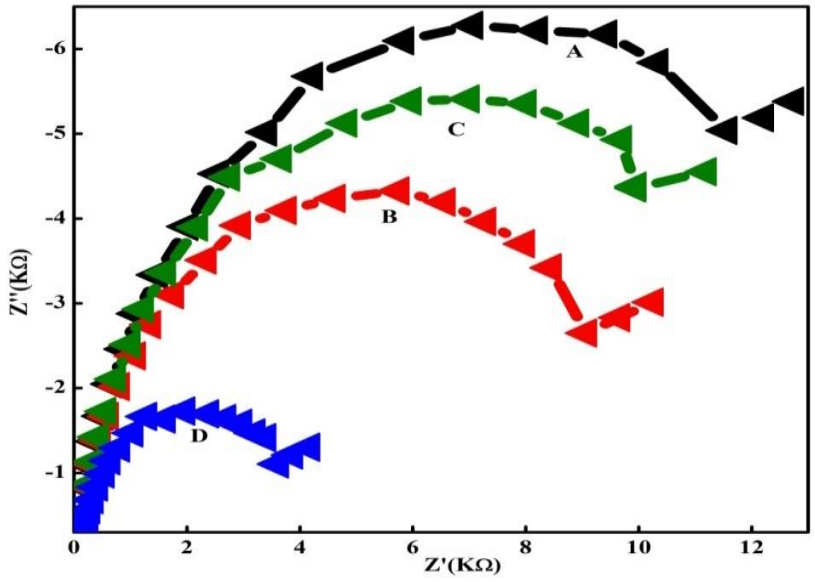

Figure 17. Nyquist impedance plots of A) PANI/ZnO, B) PANI/ZnO/CeO_2, C) PANI/g–C_3N_4/ZnO, and D) PANI/g–C_3N_4/ZnO/CeO_2 nanocomposite modified electrodes recorded in 0.1 M PBS + 0.1 M KCl solution containing 2 mM $Fe[(CN)_6]^{3-/4-}$

4.7. Electrochemical Performance of PANI/g–C_3N_4/ZnO/CeO_2 Modified Electrode

For studying the reversibility of PANI/g–C_3N_4/ZnO/CeO_2 electrode 0.1 M PBS + $K_3Fe(CN)_6$ in 0.1 M KCl was used as a redox probe. Cyclic voltammogram in a potential range from -200 to 700 mV is shown in Figure 18 and its various electrochemical parameters are evaluated and summarized in Table 3. The cyclic voltammetry curves recorded displays one oxidation and one reduction peak. As the scan rate increases the anodic and cathodic peak potentials nearly remain constant and also the difference in anodic and cathodic peak potentials falls in the range 67 – 94 mV, which conforms that the reversibility of the process (Britto *et al.*, 2011).

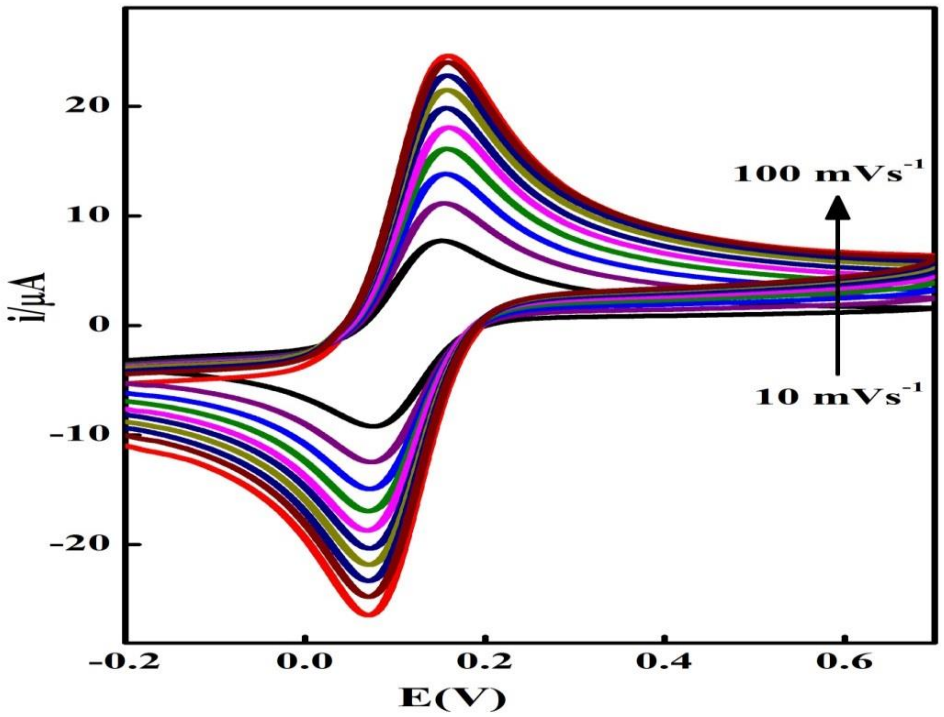

Figure 18. Cyclic voltammograms of 0.1 M PBS + 2 mM $K_3Fe(CN)_6$ + 0.1 M KCl at different scan rates (10 to 100 mVs^{-1}) on PANI/g–C_3N_4/ZnO/CeO_2/GCE.

Table 3. Electrochemical parameters of PANI/g–C_3N_4/ZnO/CeO_2 evaluated from the CV in 2.0 mM $K_3Fe(CN)_{6.}$ + 0.1 M KCl and 0.1 M PBS

Scan rate(mVs^{-1})	E_{pa}(mV)	E_{pc}(mV)	I_{pa}(µA)	I_{pc} (µA)	I_{pa}/I_{pc}	ΔEp
10	155	73	8.10	8.74	0.93	82
20	157	75	11.53	12.05	0.96	82
30	158	76	14.1	14.5	0.97	82
40	160	75	16.4	16.6	0.99	83
50	160	73	18.36	18.4	0.999	85
60	162	74	20.20	20.22	0.999	88
70	161	74	21.7	21.61	1.004	87
80	162	75	23.05	23.04	1.00	87
90	162	75	24.32	24.41	0.996	87
100	163	75	25.07	26.04	0.963	88

The electrochemical behavior of the PANI/g–C_3N_4/ZnO/CeO_2 modified electrode was investigated using cyclic voltammetry. Figure 19, represents the CV responses of the modified electrode in 0.1 M PBS + 2.0 mM $K_3Fe(CN)_{6.}$ + 0.1 M KCl at different scan rates (25 to 100 mVs^{-1}). It was found that anodic and cathodic peak currents distinctly increase with the increasing potential scan rate.

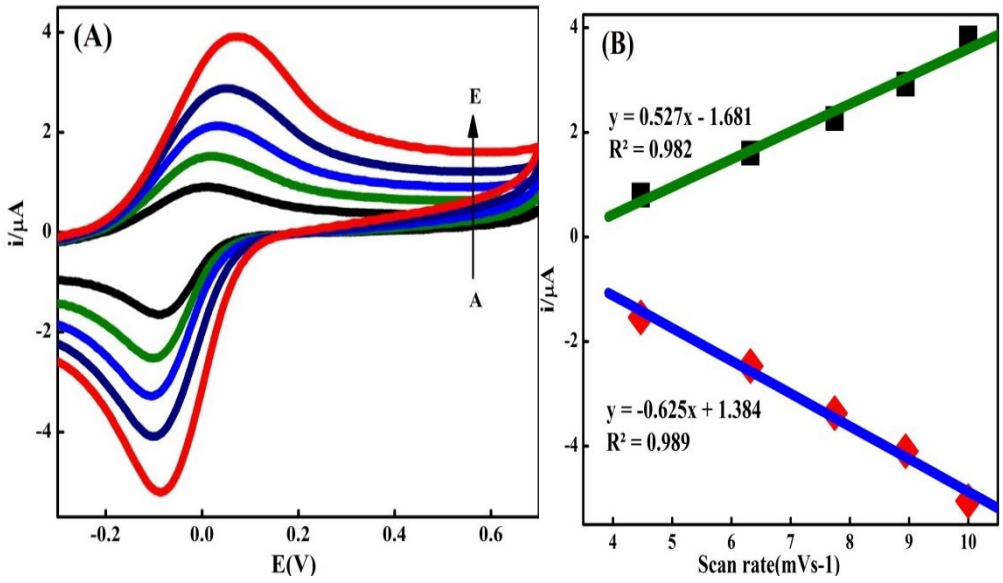

Figure 19. A) Cyclic voltammograms of PANI/g–C_3N_4/ZnO/CeO_2/GCE examined at various scan rates (A – E): 20, 40, 60, 80 and 100 mVs^{-1} in 0.1 M PBS + 2.0 mM $K_3Fe(CN)_6$ in 0.1 M KCl. B) Plot of the peak current to the square root of the scan rates.

As shown in Figure 19, the relationship of the anodic (Ipa) peak currents and cathodic peak current versus the scan rate in the range 25 to 100 mVs^{-1}, whose equation is Ipa (μA) = 0.527 x − 1.681 (R^2 = 0.982), and Ipc (μA) = − 0.625x + 1.384 (R^2 = 0.989) suggesting that a controllable adsorption process occurring at PANI/g–C_3N_4/ZnO/CeO_2/GCE. Which is ideal for detection of malathion.

4.8. Effect of pH on PANI/g–C_3N_4/ZnO/CeO_2/GCE

The effect of pH on malathion oxidation was investigated in the pH range of 4 to 8. The pH was adjusted by using 0.1 M HCl and 0.1 M NaOH. Figure 20, displays the pH dependent voltammetric response of the PANI/g–C_3N_4/ZnO/CeO_2 modified electrode and investigated in 0.1 M PBS + 2.0 mM $K_3Fe(CN)_6$ in 0.1 M KCl + 2.0 × 10^{-8} M malathion solutions from pH 4 to 8 at constant scan rate of 50 mVs^{-1}. The current signal increased with increasing solution pH value to pH 7.0, and then decreased. These results indicate that neutral conditions are suitable for the oxidation reaction. In contrast, acid and base buffer resulted in weak signal strength and poor peak shape; pH 7.0 was selected as the optimum pH for further experiment.

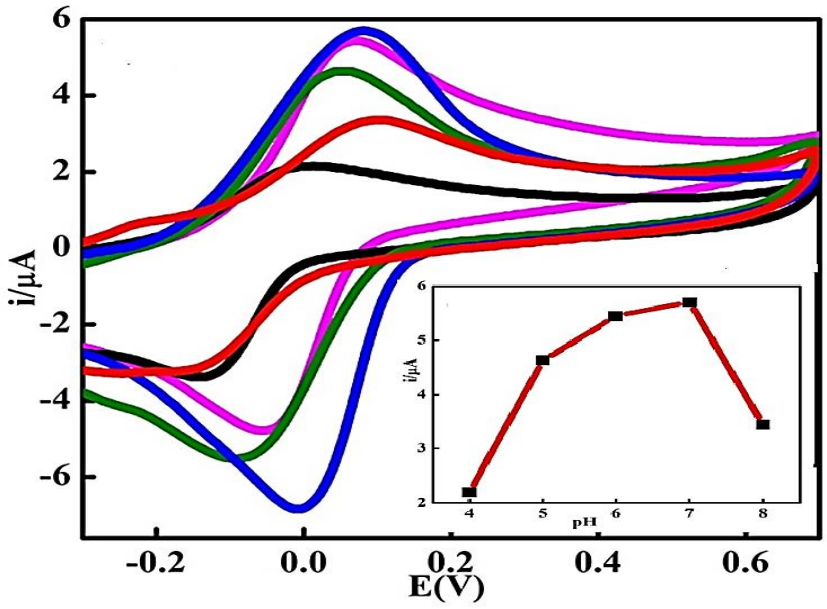

Figure 20. Cyclic voltammograms of PANI/g–C_3N_4/ZnO/CeO_2/GCE under different pH conditions (pHs 4.0, 5.0, 6.0, 7.0 and 8.0 scan rate = 50 mVs^{-1}) in 0.1 M PBS + 2.0 mM $K_3Fe(CN)_6$ in 0.1 M KCl + 2.0 × 10^{-8} M malathion. Inset: Plot of pH versus peak current.

4.9. Effect of Scan Rate on PANI/g–C_3N_4/ZnO/CeO_2/GCE

The influence of scan rate on malathion oxidation at PANI/g–C_3N_4/ZnO/CeO_2/GCE was also investigated. Figure 21, reveals the CV of 2.0 × 10^{-8} M malathion at PANI/g–C_3N_4/ZnO/CeO_2/GCE at various scan rates. The redox peaks current increased gradually with the increase of scan rate. As shown in Figure (21B), both the anodic and cathodic peak currents grew linearly with the square root of scan rate in the range of 10 to 100 mVs^{-1}. The linear relationship between the anodic peak current versus the scan rate and the cathodic peak current versus the scan rate was validated by the linear regression equations Ipa (μA) = 1.283x − 3.025(R^2 = 0.991), and Ipc (μA) = −1.298x + 2.146 (R^2 = 0.995) respectively. This result indicated that the electrooxidation of malathion on PANI/g–C_3N_4/ZnO/CeO_2/GCE is a typical diffusion controlled process and the observed CV results indicate that the prepared PANI/g–C_3N_4/ZnO/CeO_2 nanocomposite act as an efficient electron mediator for the electrochemical sensing of malathion.

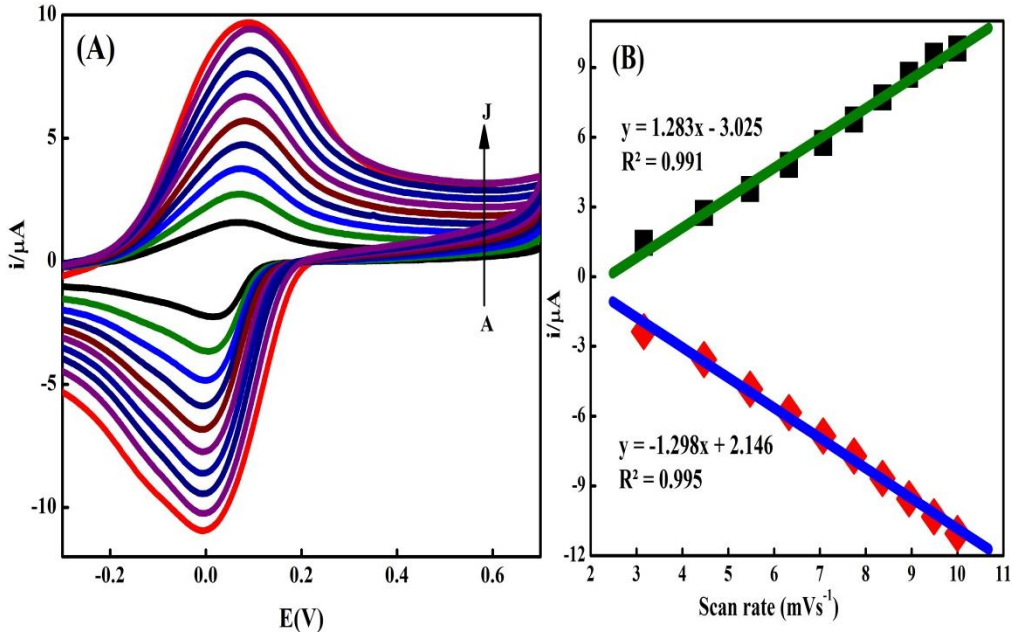

Figure 21. A) Cyclic voltammograms of the PANI/g–C_3N_4/ZnO/CeO_2 nanocomposite electrode in 2.0 × 10^{-8} M malathion + 0.1 M PBS + $K_3Fe(CN)_6$ in 0.1 M KCl at different scan rates. B) Plot of the anodic and cathodic peak currents on the PANI/g–C_3N_4/ZnO/CeO_2 nanocomposite electrode versus square root of the scan rates.

4.10. Detection of Malathion Using PANI/g–C_3N_4/ZnO/CeO_2/GCE Working Electrode

Due to the good sensitivity, differential pulse voltammetry was applied for further electrochemical detection of malathion under the optimized operating conditions. The PANI/g–C_3N_4/ZnO/CeO_2 composite electrode was used to detect malathion concentration in phosphate buffer pH 7. Figure (22), shows the DPV response of different concentrations of malathion on PANI/g–C_3N_4/ZnO/CeO_2 composite electrode. A well-defined peak was observed around + 60 mV for oxidation of malathion at PANI/g–C_3N_4/ZnO/CeO_2 composite electrode in the presence of various malathion concentrations. It is in agreement with Ebrahim *et al*. (2014) reported. Each of well-defined peaks, proportional to the concentration of the corresponding malathion was observed in plots.

The corresponding calibration plot (i_{pa} vs. C malathion) was presented in Figure 22 (Inset) to build up the calibration equation for real sample detection. The oxidation peak current of the PANI/g–C_3N_4/ZnO/CeO_2 electrode exhibits a linear dependence on malathion concentration. The linear relationship was observed for the concentration ranging from 2×10^{-8} M to 14×10^{-8} M as observed in Figure 22(B). The sensitivity of the PANI/g–C_3N_4/ZnO/CeO_2 electrode calculated from the slope of curve has been found to be 11.85 µA/µM and the correlation coefficient from the linear regression analysis for this electrode has been found to be 0.997.

The minimum concentration which is detected by PANI/g–C_3N_4/ZnO/CeO_2/GCE was calculated by using equation LOD $=\frac{3\sigma}{m}$. The standard deviation for seven measurements was found to be 0.043205 and slope (m) from the graph was found to be 11.85. Hence the minimum detection limit (LOD) in the linear range for the modified electrodes is 10.94×10^{-9} M malathion.

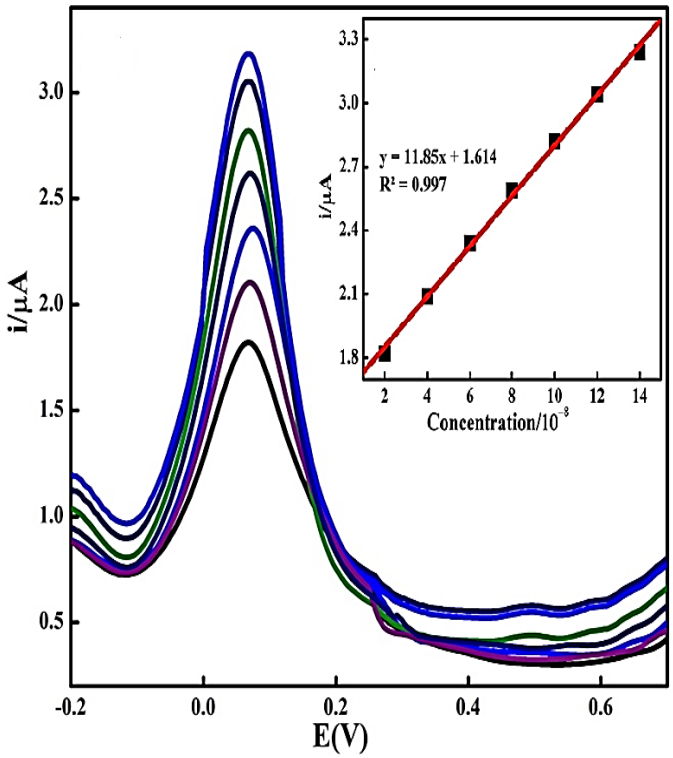

Figure 22. Differential pulse voltammeteric plot of successive addition of malathion in 0.1 M PBS + $K_3Fe(CN)_6$ in 0.1 M KCl. Inset: Plot of the anodic peak current response (Ipa) versus malathion concentration.

Table 4. Comparison of different modified electrodes for determination of Organophosphate Pesticides

Type of electrode	LOD	Technique	Reference
Au/MWCNTs/GCE	100×10^{-9} M	DPV	Zhang *et al*., 2009
PANI-Nanofibers-SWCNTs	2×10^{-7} M	DPV	Ebrahim *et al.*, 2014
AChE–SiSG–CPE	58×10^{-9} M	DPV	Raghu *et al*., 2014
Ionic liquid–graphene/GCE	6.0×10^{-8} M	DPV	Zhao *et al.*, 2013
Graphene/GCE	1.0×10^{-8} M	DPV	Liu *et al.*, 2014
CuO–SWCNTs	0.3×10^{-9} M	DPV	Huo *et al.*, 2014
PANI/g–C_3N_4/ZnO/CeO_2	10.94×10^{-9} M	DPV	This work

The detection limit obtained in this work was lower than the results from other nanomaterials based organophosphate electrochemical sensor. Such excellent sensing performance could be attributed to the high affinity between PANI/g–C_3N_4/ZnO/CeO_2 hybrid composite and malathion.

4.11. Determination of Malathion in Khat Sample

To evaluate the feasibility of the PANI/g–C_3N_4/ZnO/CeO_2 modified electrode, it was used to detect the malathion concentration in khat sample. Differential pulse voltammetric method was applied to evaluate the current response by using the standard addition method. Khat sample used in this work did not contain detectable amount of malathion, as employing the developed sensor, hence the sample was spiked with 4×10^{-8} M. From the calibration curves plotted for the known standard solution of malathion, the unknown concentration of malathion (value of X) was successfully calculated by using equation y = A + B*X obtained from the calibration curves of the standard solution. The calculated amount of malathion concentration in khat sample was 3.91×10^{-8} M.

4.12. Important Properties of PANI/g–C_3N_4/ZnO/CeO_2 Modified Electrode

4.12.1. Stability and Reproducibility of the Sensor

The stability of PANI/g–C_3N_4/ZnO/CeO_2 modified electrode was evaluated by measuring its current response to 4×10^{-8} M malathion within a 15 day period. The PANI/g–C_3N_4/ZnO/CeO_2 modified electrode was exposed to air, and its current response was tested every 3 day. The sensor showed good stability, with a loss of only approximately 14.4% in current response after 15 days.

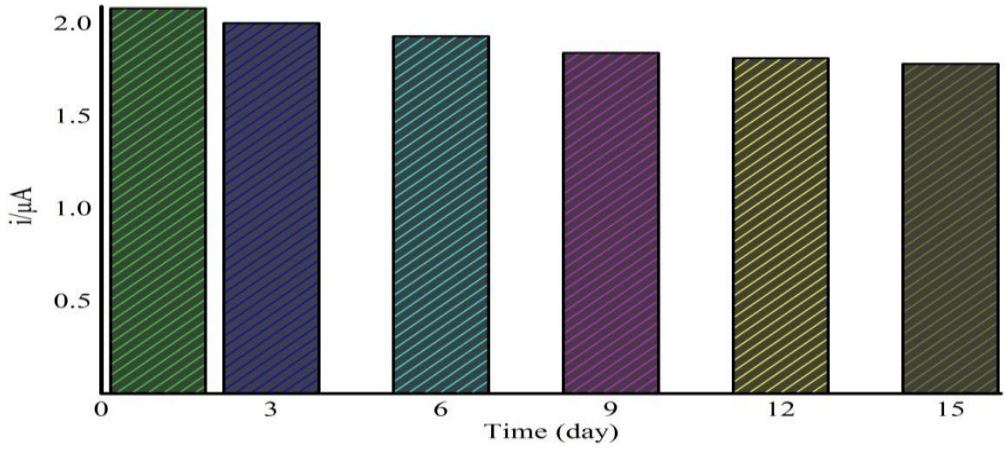

Figure 23. Stability of PANI/g–C_3N_4/ZnO/CeO_2/GC electrode in 4×10^{-8} M malathion

The PANI/g–C_3N_4/ZnO/CeO_2 modified electrode showed only 18.6% ± 2.08% decrease of the original current response after a number of 'n' days. Figure 24 indicates that the first order exponential decay response of PANI/g–C_3N_4/ZnO/CeO_2 modified electrode for 4×10^{-8} M malathion. Each corresponding values are indicated in the (Appendix Table 5).

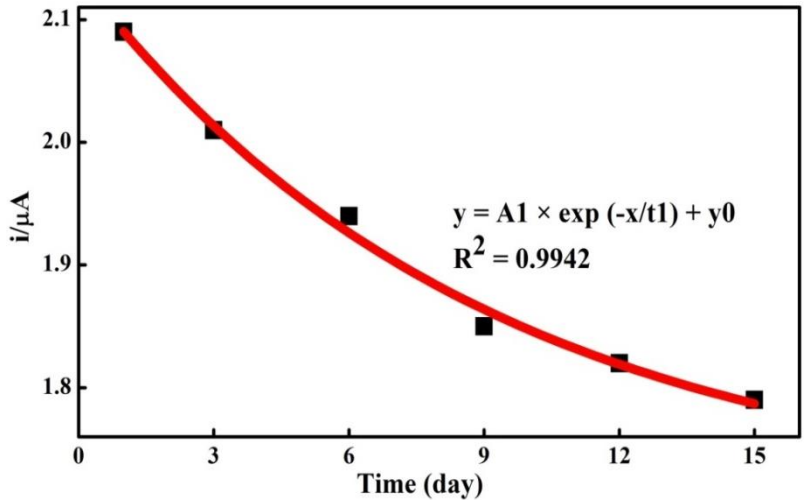

Figure 24. The variation of peak current with time along 15 days for PANI/g–C_3N_4/ZnO/CeO_2/GC in 0.1 M PBS + $K_3Fe(CN)_6$ in 0.1 M KCl + 4×10^{-8} M malathion

The reproducibility investigation for PANI/g–C_3N_4/ZnO/CeO_2 modified electrode was conducted three times (n = 3) within the same electrode. The RSD of 4.58% for 4×10^{-8} M malathion demonstrated good intra-electrode reproducibility as shown in the (Appendix Table 6). These results confirm that the PANI/g–C_3N_4/ZnO/CeO_2 modified electrode has stability as well as good reproducibility.

4.12.2. Recovery Experiment

The potential application of the proposed electrode was evaluated by malathion detection in real life samples. The malathion standard solution was added to a real life khat sample by a standard addition method. The recovery of different malathion concentrations were exhibited in Table 5 from 95.57% to 102.11%. These result indicated that the prepared electrochemical sensor had a great potential for practical applications.

Table 5. Recovery studies of spiked malathion in khat sample

Sample	Spiked	Found	Recovery (%)
1	4×10^{-8}	3.91×10^{-8}	98.3
2	6×10^{-8}	6.12×10^{-8}	102.11
3	8×10^{-8}	7.64×10^{-8}	95.57

4.12.3. Interference Analysis

Anti-interference property is an important factor for sensors. One main problem of non-enzymatic sensors is the interference from other pesticide, organic compounds and inorganic ions in real sample, which can be oxidized at potential comparable to malathion. DPV were performed with 0.1 M phosphate buffer solution + 2 mM potassium ferrocyanide in 0.1 M potassium chloride pH 7 which containing 4×10^{-8} M malathion in the absence and presence of 1000 ppb of CO_3^{2-}, SO_4^{2-}, PO_4^{3-}, NO_3^- , K^+, Na^+, Fe^{2+}, Pb^{2+}, Co^{2+}, Zn^{2+} , glucose and Carbendazim was investigated. The peak current compared with that for 4×10^{-8} M malathion were shown in the figure below

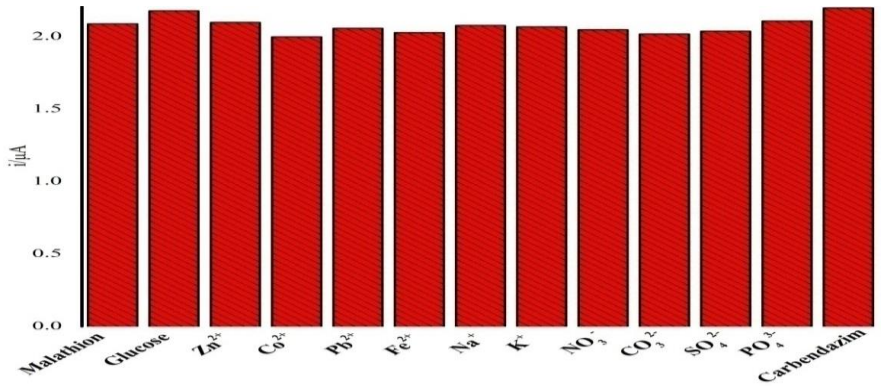

Figure 25. Selectivity studies of PANI/g–C_3N_4/ZnO/CeO_2/GCE electrode

The peak currents for the co-existence of 4×10^{-8} M malathion with other pesticide (1000 ppb of carbendazim), inorganic ions (1000 ppb of CO_3^{2-}, SO_4^{2-}, PO_4^{3-}, NO_3^- , K^+, Na^+, Fe^{2+}, Pb^{2+},Co^{2+}, Zn^{2+}), and glucose were examined. All these result indicates that there is no significant interference. This demonstrates good selectivity of the developed PANI/g–C_3N_4/ZnO/CeO_2 sensor.

5. SUMMARY, CONCLUSION AND RECOMMENDATION

5.1. Summary and Conclusion

In this work, PANI/ZnO and PANI/g–C_3N_4/ZnO, PANI/ZnO/CeO_2, and PANI/g–C_3N_4/ZnO/CeO_2 nanomaterials were successfully prepared and all the synthesized samples structural and morphological properties were characterized by XRD, UV-Vis, FTIR, SEM, TGA, BET. All these characterizations revealed that the ternary nanocomposite (PANI/g–C_3N_4/ZnO/CeO_2) posse's small crystal size (21.86 nm), small band gap (2.75 eV), high electron transfer capability and high surface area (29.778 m^2g^{-1}).

On the other hand, the electrochemical properties of GC electrode modified by PANI/ZnO, PANI/ZnO/CeO_2, PANI/g–C_3N_4/ZnO, and PANI/g–C_3N_4/ZnO/CeO_2 were investigated by CV and EIS in the presence of 0.1 M phosphate buffer solution + 2 mM potassium ferrocyanide in 0.1 M potassium chloride. Among all the modified electrodes PANI/g–C_3N_4/ZnO/CeO_2/GCE showed a high peak current and low charge transfer resistance as evaluated from CV and EIS data. The fact that PANI and g–C_3N_4 contributes to the high conductive and the catalytic role of both CeO_2 and ZnO synergistically improve the electrochemical performance. This is the reason for PANI/g-C_3N_4/ZnO/CeO_2/GCE exhibiting high electrocatalytic activity towards oxidation of malathion and these novel properties of modified electrode indicated its potential for sensor applications.

The developed PANI/g–C_3N_4/ZnO/CeO_2/GCE sensor before applied for the determination of malathion, experimental parameters pH of the PBS and scan rate were optimized. Using optimized conditions (pH = 7 and ν = 50 mVs^{-1}) the electrode was applied for the determination of malathion in standard solution (2×10^{-8} to 14×10^{-8} M) with differential pulse voltammetry. The sensor showed a linear range of 2×10^{-8} to 14×10^{-8} M, high sensitivity, 11.85 µA/µM and low detection limit of 10.94×10^{-9} M (S/N = 3). The same electrode was employed to detect the concentration of malathion in khat samples. The sample did not have detectable amount and therefore spiked with 4×10^{-8} M of malathion. Besides, the electrode possesses high stability, good intra-electrode reproducibility and good recovery value. Furthermore, the sensor was not affected by interferences that aroused from other pesticide, organic compounds and inorganic ions. The main reason was ascribed to high

conductivity of the PANI/g–C_3N_4/ZnO/CeO_2 and larger surface area due to the nanoparticles which enhanced the efficiency of the electron transfer between the electrode and the analyte. The study demonstrated that PANI/g–C_3N_4/ZnO/CeO_2/GCE developed sensor has a potential application to be used as non-enzymatic determination of malathion in various environmental samples.

5.2. Recommendation

Based on this study the following are recommended for future research.

- This study can be used as a baseline for further research on sensor based on nanocomposite modified electrodes for the detection of organophosphorus insecticides.
- To identify the best composition for the detection of malathion investigating electrochemical properties of electrode at various composition of polyaniline, zinc oxide, cerium dioxide and carbon nitride is recommended.
- To improve the stability of the sensor incorporation of binders such as nafion and using other metal oxide nanoparticles are potential areas for future research.

6. REFERENCES

Aardema, F., Radomsky, A. S., O'Connor, K. and Julien, D. 2008. Inferential confusion, obsessive beliefs and obsessive-compulsive symptoms: A multidimensional investigation of cognitive domains. *Clinical Psychology and Psychotherapy,* 15: 227–238.

Ahmad, N., Umar, A., Kumar R. and Alam, M. 2016. Microwave-assisted synthesis of ZnO doped CeO_2 nanoparticles as potential scaffold for highly sensitive nitroaniline chemical sensor. *Ceramic International,* 11: 115621–1567.

Ai, L., Jiang, J. and Zhang, R. 2010. Uniform polyaniline microspheres: A novel adsorbent for dye removal from aqueous solution. *Synthetic Metals,* 160: 762–767.

Ameen, S., Park, R., Akhtar, S.M. and Shin, S.H. 2016. Lotus-leaf like ZnO nanostructures based electrode for the fabrication of ethyl acetate chemical sensor. *Materials Letters*, 164: 562–566.

Ansari, A.A., Solanki, P.R. and Malhotra, B.D. 2009. Hydrogen peroxide sensor based on horseradish peroxidase immobilized nanostructured cerium oxide film. *Journal of Biotechnology*, 142: 179–184.

Aragay, G., Pons, J. and Merkoci, A. 2011. Recent trends in macro, micro, and nanomaterial based tools and strategies for heavy metal detection. *Chemistry Reveiw*, 111: 3433–3458.

Atta, N.F., Galal, A. and Ads, E.E. 2014. Smart Electrochemical Morphine Sensor Using poly(3,4- ethylene-dioxythiophene)/Gold-nanoparticles Composite in Presence of Surfactant. *International Journal of Electrochemical Science,* 9: 2113 – 2131.

Bakirci, G. T. and Hisil, E. 2011. Evaluation and applications in food analysis. *Food Chemistry*, 135: 1901–1913.

Bird, S.B., Sutherland,T.D., Gresham,C.,Oakeshott,J., Scott, C. and Eddleston, M. 2008. A bacterial organophosphorus hydrolase, prevents lethality in rats after with highly toxic organophosphorus pesticides. *Toxicology*, 247(2): 88 -92.

Bisetty, K., Sabela, M.I., Khulu, S., Xhakaza, M. and Ramsarup, L. 2011. Multivariate optimization of voltammetric parameters for the determination of total polyphenolic content in wine samples using an immobilized biosensor. *International Journal of Electrochemical Science,* 6: 3631 – 3643.

Bolognes, C. 2003. Genotoxicity of pesticides: a review of human biomonitoring studies. *Mutation Research,* 543: 251–272.

Britto, P.J. Santhanam, K.S.V, Ajayan, P.M. 2011. Carbon nanotube electrode for oxidation of dopamine. *Bioelectrochemistry and Bioenergetics*, 41: 121-125.

Chaudhari, H.K. and Kelkar, D.S. 1996. X-ray Diffraction Study of Doped Polyaniline. *Journal of Applied Polymer Science,* 62: 15-18.

Chen, C., Qian, Y., Chen, Q., Tao, C. and Li, C. 2011. Evaluation of pesticide residues in fruits and vegetables from Xiamen, China. *Food Control,* 22: 1114–1120.

Chen, K. Y., Janz, K.F., Zhu, W. and Brychta, R.J. 2012. Redefining the roles of sensors in objective physical activity monitoring. *Medicine and Science in Sports and Exercise,* 44: 13–12.

Chen, S., Li, S. and Thangamuthu, R. 2009. Electrochemical Preparation, Characterization, and Electrocatalytic Properties of $OsPtCl_6$ Film Electrodes Towards Reduction of NAD^+, Chloroacetic Acids, and Nitrous Oxide. *Electroanalysis,* 21: 1505-1513.

Cheng, N., Tian, J., Liu, Q., Ge, C., Qusti, H.A., Abdullah M. Asiri, M.A., Al-Youbi, O.A. and Xuping, Sun. 2013. Au-Nanoparticle-Loaded Graphitic Carbon Nitride Nanosheets: Green Photocatalytic Synthesis and Application toward the Degradation of Organic Pollutants. *Applied Materials and Interfaces*, 5: 6815−6819.

Demirtas, C., Yilmaz, S., Saglikoglu, G. and Sadikoglu, M. 2015. Electrochemical Determination of Phenazopyridine Hydrocloride using Poly(p-Aminobenzene Sulfonic Acid) Film Modified Glassy Carbon Electrode. *International Journal of Electrochemical Science,* 10: 1883–1892.

Desai, R., Mankad, V., Gupta, S.K. and Jha, P.K. 2012. Size distribution of silver nanoparticles: UV-visible spectroscopic assessment. *Nanoscience and Nanotechnology Letters*, 4: 30-34.

Ebrahim, S., El-Raey, R., Hefnawy, A., Ibrahim, H., Soliman, M. and Abdel-Fattah, T.M. 2014. Electrochemical sensor based on polyaniline nanofibers/single wallcarbon nanotubes composite for detection of malathion. *Synthetic Metals,* 190: 13–19.

Faraji, Y. Yamini and M. Rezaee. 2010. Magnetic Nanoparticles: Synthesis, Stabilization, Functionalization, Characterization, and Applications. *Journal of Iranian Chemical Society*, 7(1): 1-37.

Farghaly, O.A., Hameed, R.S. and Newwas, A.A. 2014. Analytical Application Using Modern Electrochemical Techniques. *International Journal of Electrochemical Science,* 9: 3287 – 3318.

FEPA (The Federal Environmental Protection Authority). 2004. Environmental Impact Assessment Guideline on Pesticides. FEPA, Addis Ababa, Ethiopia.

Genies, E. M.; Boyle, A.; Lapkowski, M. and Tsintavis, C. 1990. Polyaniline: A historical survey. *Synthetic Metals,* 36: 139-182.

Ghanbari, K. and Babaei, Z. 2016. Fabrication and characterization of non-enzymatic glucose sensor based on ternary NiO/CuO/polyaniline nanocomposite. *Analytical Biochemistry,* 498: 37-46.

Goharshadi, E.K., Samiee, S. and Nancarrow, P. 2011. Fabrication of cerium oxide nanoparticles: Characterization and optical properties. *Journal of Colloid and Interface Science,* 356: 473–480.

Groenewolt, M. and Antonietti, M. 2005. Synthesis of g–C_3N_4 nanoparticles in mesoporous silica host matrices. *Advanced Materials,* 17: 14-17.

Guan, H., Brewer, W. E. and Garris, S. T. 2010. Disposable pipette extraction for the analysis of pesticides in fruit and vegetables using gas chromatography/mass spectrometry. *Journal of Chromatography A,* 1217: 1867-1874.

Haber, J., Block, J. H. and Delmon, B.1995. Manual of methods and procedures for catalyst characterization (Technical Report). *Pure and Applied Chemistry*, 67(8/9): 1257-1306.

Hamdy, A.S., Shenawy, E. and Bitar, T.E. 2006. Electrochemical impedance spectroscopy study of the corrosion behavior of some niobium bearing stainless steels in 3.5% NaCl. 2006. *International Journal of Electrochemical Science,* 1: 171-180.

Hanrahan, G., Patil, D.G. and Wang, J. 2004. Electrochemical sensors for environmental monitoring: design, development and applications. *Journal of Environmental Monitoring,* 6(8): 657-664.

Hasanpoor, M., Aliofkhazraei, M. and Delavari, H. 2016. In-situ study of mass and current density for electrophoretic deposition of zinc oxide nanoparticles. *Ceramics International,* 42: 6906-6913.

Hasoon, S.A. and Sally Hadi, AA. 2018. Optical, Structural and Electrical Properties of Electrochemical Synthesis of Thin Film of Polyaniline. *Open Access Baghdad Science Journal,* 15(1): 73-80.

He, Y., Wang, Y., Zhang, L., Teng, B. and Fan, M. 2015. High-efficiency conversion of CO_2 to fuel over ZnO/g–C_3N_4 photocatalyst. *Applied Catalysis B: Environmental*, 168: 1–8.

Hernández, A.J., Manzanares, V.M., Ortiz, G.R., Carlos, H.B., Torres, P.M. and de-Alba, L.L. 2005. Simultaneous Spectrophotometric Determination of Atrazine and Dicamba in Water by Partial Least Squares Regression. *Journal of Chilean Chemical Society*, 50(2): 461-464.

Hu, J. and Zhou, Y. 2016. The properties of nano(ZnO-CeO_2)@polysiloxane core–shell microspheres and their application for fabricating optical diffusers. *Applied Surface Science,* 365: 166–170.

Huo, D., Li, Q., Zhang,Y., Hou, C. and Lei, Y. 2014. A highly efficient organophosphorus pesticides sensor based on CuO nanowires–SWCNTs hybrid Nanocomposite. *Sensors and Actuators B*, 199: 410–417.

Jia, X., Dai, R., Sun, Y., Song, H. and Wu., x. 2016. One-step hydrothermal synthesis of Fe_3O_4/g–C_3N_4 nanocomposites with improved photocatalytic activities. *Journal of Material Science,* 27:3791–3798.

Jo, W.K. and Selvam, N.C. 2015. Enhanced visible light-driven photocatalytic performance of ZnO–g–C_3N_4 coupled with graphene oxide as a novel ternary nanocomposite. *Journal of Hazardous Materials*, 299:462–470.

Keshmiri, M., Troczynski, T. and Mohseni, M. 2006. Properties of amorphous and crystalline titanium dioxide from first principles. *Journal of Hazardous Materials,* 128: 130-137.

Khan, S.B., Faisal, M., Rahman, M.M. and Jamal, A. 2011. Exploration of CeO_2 nanoparticles as a chemi-sensor and photo-catalyst for environmental applications. *Science of the Total Environment*, 409: 2987–2992.

Lamba, R., Umar, A., Mehta, S.K. and Kansal, S.K. 2015. CeO_2/ZnO hexagonal nanodisks: Efficient material for the degradation of direct blue 15 dye and its simulated dye bath effluent under solar light. *Journal of Alloys and Compounds,* 620:67–73.

Leandro, K.C., Carvalho, J.D., Giovanelli1, L.F. and Moreira, J.C. 2009. Development and validation of an electroanalytical methodology for determination of isoniazid and rifampicin content in pharmaceutical formulations. *Brazilian Journal of Pharmaceutical Sciences,* 45: 331-337.

Li, G. and Miao, P. 2012. Theoretical Background of Electrochemical Analysis. *Electrochemical Analysis of Proteins and Cells*, 5-18.

Li, X., Li, M., Yang, J., Li, X., Hu, T., Wang, J., Sui, Y., Wu, X. and Kong, L. 2014. Synergistic effect of efficient adsorption g–C_3N_4/ZnO composite for photocatalytic property. *Journal of Physics and Chemistry of Solids,* 75: 441–446.

Liu, S., Yuan, L., Yue, X., Zheng, Z. and Tang, Z. 2008. Recent advances in nanosensors for organophosphate pesticide detection. *Advanced Powder Technology,* 19: 419-441.

Liu, X., Song, B., and Wang, Y. Z. 2014. Determination of residual parathion based on the graphene modified glassy carbon electrode. *China Journal of Analytical Science*, 30: 509–512.

Malinauskas, A., Malinauskiene, J. and Ramanavičius, A. 2005. Conducting polymer based nanostructurized materials: electrochemical aspects. *Nanotechnology,* 16(10): 51-62.

Mostafa, G. 2010. Electrochemical Biosensors for the Detection of Pesticides. *The Open Electrochemistry Journal,* 2: 22-42.

Musić, S., Popovic, S., Maljković, M. and Dragčević, D. 2002. Influence of synthesis procedure on the formation and properties of zinc oxide. *Journal of Alloys and Compounds,* 347: 324-332.

O'Donoghue, M. 1983. A guide to Man-made Gemstones. pp. 40-44. Van Nostrand Reinhold Company, Great Britain.

Pérez-López, B. and Merkoci, A. 2011. Nanomaterials Based Biosensors for Food Analysis Applications. *Trends in Food Science and Technology*, 22(11): 625-639.

Plata, M.R.,Contento, A.M. and Ríos, A. 2010. State of the Art of (Bio)Chemical Sensor Developments in Analytical Spanish Groups. *Sensors*, 10(4): 2511–2576.

Pradier, C.M., Rubio, C., Poleunis, C., Bertrand, P. and Marcus, P. 2005. Surface Characterisation of Three Marine Bacterial Strains by FT-IR, XPS and ToF-SIMS, Correlation with Adhesion on Stainless Steel Surfaces. *Journal of Physical Chemistry,* 4: 336-344.

Prompheta, N., Rattanarat, P., Rangkupan, R., Chailapakul, O. and Rodthongkum, N. 2015. An electrochemical sensor based on graphene/polyaniline/polystyrene nanoporous fibers modified electrode for simultaneous determination of lead and cadmium. *Sensors and Actuators B:* 207:526-534.

Qin, J., Yang. C., Cao. M., Zhang, X., Rajendran, S., Limpanart, S., Ma, M. and Liu, R. 2016. Two-dimensional porous sheet-like carbon-doped ZnO/g–C_3N_4 nanocomposite with high visible light photocatalytic performance. *Materials Letters,* 189:156–159.

Rades, S., Hodoroaba, V.D., Salge, T., Wirth, T., Lobera, M.P., Labrador , R.H., Natte, K., Behnke, T., Gross, T. and Unger, W.E. 2014. High-resolution imaging with SEM/T-SEM, EDX and SAM as a combined methodical approach for morphological and elemental analyses of single engineered nanoparticles. *Royal Society of Chemistry,* 4: 49577-49587.

Raghu, P., Reddy, T.M., Reddaiah, K., Swamy, B.E.K. and Sreedhar, M. 2014. Acetylcholinesterase based biosensor for monitoring of malathion and acephate in food samples: A voltammetric study. *Food Chemistry*, 142: 188–196.

Rogers, R.K. 1995. Biosensors for environmental applications. *Biosensors and Bioelectronics*,10 (6): 533-541.

Rong, X., Qiu, F., Jiang, Z., Rong, J., Pan, J., Zhang, T. and Yang. D. 2016. Preparation of ternary combined ZnO-Ag_2O/porous g–C_3N_4 composite photocatalyst and enhanced visible-light photocatalytic activity for degradationof ciprofloxacin. *Chemical Engineering Research and Design,* 3: 253–261.

Ronkainen, N.J., Halsallb, H.B. and Heinemanb, W.R. 2010. Electrochemical biosensors. *Chemical Society Reviews*, 39: 1747-1763.

Ruecha, N., Rodthongkum, N., Cate, D.M., Volckens, J., Chailapakul, O. and Henry, C.H. 2015. Sensitive electrochemical sensor using a graphene–polyaniline nanocomposite for simultaneous detection of Zn(II), Cd(II), and Pb(II). *Journal of Chemical Engineering,* 874: 40–48.

Ryu, S.K., Kim, M.K., Park, G.N., Park, J.Y. and Chang, H.S. 2002. Hydrophilic polyaniline nanofibrous architecture using electrosynthesis method for supercapacitor application. Journal of Power Source, 103: 305-309.

Saboor, H.F., Khodadadi, A.K., Mortazavi, Y. and Asgari, M. 2017. Microemulsion synthesized silica/ZnO stable core/shell sensors highly selective to ethanol with minimum sensitivity to humidity. *Sensors and Actuators B,* 238: 1070–1083.

Shamsipur, M., Karimi, Z. and Tabrizi, M.A. 2015. A highly sensitive hydrogen peroxide sensor based on (Ag–Au NPs)/poly[o-phenylenediamine] modified glassy carbon electrode. *Materials Science and Engineering C,* 56: 426-431.

Sierra, M., Borges, E., Esparza, P., Méndez-Ramos, J., Jesús Martín-Gil, J. and Martín-Ramos, P. 2016. Photocatalytic activities of coke carbon/g–C_3N_4 and Bi metal/Bi mixed oxides/g–C_3N_4 nanohybrids for the degradation of pollutants in wastewater. *Science and Technology of Advanced Materials*, 17(1): 659–668.

Simsíková, M., Cechal, J., Zorkovská, A., Antalík, M. and Sikola, T. 2014. Preparation of CuO/ZnO nanocomposite and its application as a cysteine/homocysteine colorimetric and fluorescence detector. *Colloids and Surfaces B,* 123: 951–958.

Singh, K., Ibrahim, A.A., Umar, A., Kumar, A., Chaudhary, A.G., Singh, S. and Mehta, K.S. 2014. Synthesis of CeO_2–ZnO nanoellipsoids as potential scaffold for the efficient detection of p-nitrophenol, *Sensors and Actuators B*, 202: 1044–1050.

Stradiotto, N.R., Yamanaka, H. and Zanoni, M.V. 2003. Electrochemical Sensors: A Powerful Tool in Analytical Chemistry. *Journal of the Brazilian Chemical Society*, 14:159-173.

Thirumavalavan, M., Huang, K.L. and Lee, J.F. 2013. Preparation and Morphology Studies of Nano Zinc Oxide Obtained Using Native and Modified Chitosans. *Materials*, 6(9): 4198-4212.

Tian, J., Liu, Q., Asiri, A.M., Qusti, A.H., Al-Youbicd, A.O. and Sun, X. 2013. Ultrathin graphitic carbon nitride nanosheets: a novel peroxidase mimetic, Fe doping-mediated catalytic performance enhancement and application to rapid, highly sensitive optical detection of glucose. *Nanoscale*, 5: 11604.

Waheed, A. Badawy, W.A., Ismail, K.M. and Medany, S.S. 2011. Polyaminoanthraquinone Modified Electrodes as Electroanalytical Sensors. *International Journal of Electrochemical Science,* 6: 4204 – 4217.

Wang, J. and Zhang, D.W. 2012. Modification of TiO_2 nanorod arrays by graphite-like C_3N_4 with high visible light photoelectrochemical activity. *Electrochimica Acta,* 71: 10–16.

Wang, B., Huan, T.H., Zheng, Q.Z., Zhou, H.Y. and Gao, C. 2017. Low-temperature and highly sensitive C_2H_2 sensor based on Au decorated ZnO/In_2O_3 belt-tooth shape nano-heterostructures. *Sensors and Actuators B*, 244: 344–356.

Wanner, B.L. and Metcalf, W.W. 1992. Molecular genetic studies of a 10.9-kb operon in Escherichia coli for phosphonate uptake and biodegradation. *Federation of European Microbiological Societies Letters*, 100: 133-139.

Wu, X., Han, Y., Zhang, X., Zhou, Z. and Lu, C. 2016. Large-Area Compliant, Low-Cost, and Versatile Pressure-Sensing Platform Based on Microcrack-Designed Carbon Black @ Polyurethane Sponge for Human–Machine Interfacing. *Advanced Functional Materials*, 26(34): 6246-6256.

Xiao, X., Luan, Q., Yao, X. and Zhou, K. 2009. Single-crystal CeO_2 nanocubes used for the direct electron transfer and electrocatalysis of horseradish peroxidase. *Biosensors and Bioelectronics*, 24: 2447–2451.

Xu, H., Yan, J., Xu, Y., Song, Y., Li, H., Xia, J., Huang, C. and Wan, H. 2012. Novel visible-light-driven AgX/graphite-like C_3N_4 (X= Br, I) hybrid materials with Synergistic photocatalytic activity. *Applied Catalysis B: Environmental*, 129: 182–193.

Xu, H., Zhu, X., Dong, Y., Wu, H., Chen, Y. and Chi, Y. 2016. Highly sensitive electrochemiluminescent sensing platform based on graphite carbon nitride nanosheets for detection of pyrophosphate ion in the synovial fluid. *Sensors and Actuators B: Chemical*, 236(29): 8-15.

Yuana, Y., Huanga, G.F., Hub, W.Y., Xionga, D.N., Zhoua, B.X., Changc, S. and Huang, W.Q. 2017. Construction of g−C_3N_4/CeO_2/ZnO ternary photocatalysts with enhanced photocatalytic performance. *Journal of Physics and Chemistry of Solids*, 106: 1–9.

Zhai, J., Wang, T., Wang, C. and Liu, D. 2018. UV-light-assisted ethanol sensing characteristics of g-C_3N_4/ZnO composites at room temperature. *Applied Surface Science*, 441: 317–323.

Zhang, L. and Fang, M. 2010. Nanomaterials in pollution trace detection and environmental improvement. *Nano Today*, 5(2): 128-142.

Zhang, J., Bi, H., He, G., Zhou, Y., Chen, H. 2014. Fabrication of Ag_3PO_4−PANI−GO, composites with high visible light photocatalytic performance and stability. *Journal of Environmental Chemical Engineering*, 2: 952-957.

Zhang, W., Xie, G., Li, S., Lu, L. and Liu. B. 2012. Au/CeO_2–chitosan composite film for hydrogen peroxide sensing. *Applied Surface Science*, 258: 8222–8227.

Zhang, Y., Kang, T.F. Wan, Chen, S.Y. 2009. Gold nanoparticles-carbon nano-tubes modified sensor for electrochemical determination of organophosphatepesticides. *International Journal of Chemical Science and Technology,* 165: 307–311.

Zhao, J., Zhang, C.C., Wang, D.B., 2015. A facile one-step synthesisof p-CuO/n-ZnO nanowire heterojunctions by thermal oxidation route. *Materal Science of Semiconductor Process,* 35: 55–58.

Zhao, L. J., Zhao, F. Q. and Zeng, B. Z. 2013. Electrochemical determination of methyl parathion using a molecularly imprinted polymer– ionic liquid–graphene composite film coated electrode. *Sensor and Actuators B,* 176: 818–824.

Zhou, N.D., Wang. J., Chen, T., Yu, Z.G. and Li, G.X. 2006. Enlargement of gold nanoparticles on the surface of a self-assembled monolayer modified electrode: a mode in biosensor design. *Analytical Chemistry,* 78(14):5227–5230.

7. APPENDICES

Appendix Table 1. Cyclic voltammograms of PANI/g-C_3N_4/ZnO/CeO_2/GCE examined at various scan rates (A – E): 20, 40, 60, 80, and 100 mVs^{-1} in 0.1 M PBS

Scan rate($mV\ s^{-1}$)	E_{pa}(mV)	E_{pc}(mV)	I_{pa}(μA)	I_{pc} (μA)	I_{pa}/I_{pc}	ΔEp
20	94	4	1.07	1.4	0.76	100
40	106	5	1.68	2.2	0.76	101
60	127	8	2.30	2.9	0.77	119
80	140	15	3.10	3.8	0.82	125
100	160	30	4.10	4.9	0.84	130

Appendix Table 2. Cyclic voltammograms of the PANI/g-C_3N_4/ZnO/CeO_2 nanocomposite electrode in 2×10^{-8} M malathion + 0.1 M PBS at different scan rates

Scan rate(mVs^{-1})	E_{pa}(mV)	E_{pc}(mV)	I_{pa}(μA)	I_{pc} (μA)	I_{pa}/I_{pc}	ΔEp
10	163	101	1.8	-2.01	0.89552	62
20	165	101	3.04	-3.29	0.92401	64
30	168	100	4.0	-4.40	0.90909	68
40	168	99	4.98	-5.50	0.90545	69
50	169	99	6.01	-6.48	0.92747	70
60	170	98	6.9	-7.3	0.94521	72
70	172	98	7.93	-8.2	0.96707	74
80	174	98	8.8	-9.1	0.96703	76
90	175	98	9.65	-9.9	0.97475	77
100	177	98	9.93	-10.6	0.93679	79

Appendix Table 3. Electrochemical parameters evaluated form the DPV of different concentration of malathion for PANI/g-C_3N_4/ZnO/CeO_2

Consentration of Malathion(M)	I_{pc} (μA)
2 × 10-8	1.82
4 × 10-8	2.09
6 × 10-8	2.34
8 × 10-8	2.59
10 × 10-8	2.82
12 × 10-8	3.04
14 × 10-8	3.24

Appendix Table 4. Stability investigation for PANI/g-C_3N_4/ZnO/CeO_2 modified electrode

Time (day)	i/µA	% Response
1	2.09	100.00
3	2.01	96.17
6	1.94	92.82
9	1.85	88.52
12	1.82	87.10
15	1.79	85.65

Appendix Table 5. Stability investigation for PANI/g-C_3N_4/ZnO/CeO_2 modified electrode for 'n' number of days

Corresponding values	Equation	Regration value
y_0= 1.70629±0.04362 A_1= 0.42917±0.03582 t_1= 8.97884±2.00983	$y = A_1*\exp(-x/t_1) + y_0$	$R^2 = 0.9942$

Appendix Table 6. Reproducibility investigation for PANI/g-C_3N_4/ZnO/CeO_2 modified electrode compared with standard malathion concentration of 4×10^{-8} M

Trial	I_{pc} (µA)	% Detection	% RSD
1	2.13	102	
2	2.01	96	4.6
3	1.94	93	